

The Effective Temperatures and Physical Properties of Magellanic Cloud Red Supergiants: The Effects of Metallicity

Emily M. Levesque^{1,2}, Philip Massey²

Lowell Observatory, 1400 W. Mars Hill Road, Flagstaff, AZ 86001

emsque@mit.edu, Phil.Massey@lowell.edu

K. A. G. Olsen²

*Cerro Tololo Inter-American Observatory, National Optical Astronomy Observatory,
Casilla 603, La Serena, Chile*

kolsen@noao.edu

Bertrand Plez

*GRAAL CNRS UMR5024, Université de Montpellier II, 34095 Montpellier Cedex 05,
France*

Bertrand.Plez@graal.univ-montp2.fr

Georges Meynet and Andre Maeder

Geneva Observatory, 1290 Sauverny, Switzerland

georges.meynet@obs.unige.ch, andre.maeder@obs.unige.ch

ABSTRACT

We present moderate-resolution optical spectrophotometry of 36 red supergiants (RSGs) in the LMC and 39 RSGs in the SMC. Using the MARCS stellar atmosphere models to fit this spectrophotometry, we determine the reddenings, effective temperatures and other physical properties, such as bolometric luminosity and effective stellar radii, and compare these to stellar evolutionary models.

¹Current address: Massachusetts Institute of Technology, 77 Massachusetts Avenue, Cambridge, MA 02139.

²Visiting Astronomer, Cerro Tololo Inter-American Observatory (CTIO), National Optical Astronomy Observatory (NOAO), which is operated by the Association of Universities for Research in Astronomy (AURA), Inc., under cooperative agreement with the National Science Foundation (NSF).

As a self-consistency check, we also compare the broad-band colors $(V - K)_0$ and $(V - R)_0$ with the models. The $(V - R)_0$ results are in good agreement with those from fitting the optical spectrophotometry, but the $(V - K)_0$ results show metallicity-dependent systematic differences, amounting to 3-4% in effective temperature, and 0.2 mag in bolometric luminosity, at the metallicity of the SMC; we conclude that this is likely due to the limitations of static 1D models, as spectra of RSGs in the optical and IR may reflect different atmospheric conditions due to the large surface granulation present in these stars. We adopt the scales indicated by the optical spectrophotometry and $(V - R)_0$ colors, but accept that there is still some uncertainty in the absolute temperature scales. We find that the effective temperature scales for the LMC and SMC K-type supergiants agree with each other and with that of the Milky Way, while for M-type supergiants the scales are cooler than the Galactic scale by 50 K and 150 K, respectively. This is in the sense that one would expect: since the spectral classification of RSGs is based on the line strengths of TiO, stars with lower abundances of these elements have to be cooler in order to have the same strength. However, this effect is not sufficient to explain the shift in average RSG spectral type between the three galaxies. Instead, it is the effect that metallicity has on the coolest extent of the evolution of a star that is primarily responsible. Our new results bring the RSGs into much better agreement with stellar evolutionary theory, although the SMC RSGs show a considerably larger spread in effective temperatures at a given luminosity than do the LMC stars. This is expected due to the larger effects of rotational mixing in lower-metallicity stars, as higher helium abundance at the surface would lead to higher effective temperatures in the RSG phase. We also find that the distribution of reddening of RSGs in the Clouds is skewed significantly towards higher values, consistent with our recent finding that Galactic RSGs show extra extinction due to circumstellar dust.

Subject headings: stars: atmospheres—stars: fundamental parameters—stars:late-type—supergiants—dust, extinction

1. Introduction

Until recently, the location of Galactic red supergiants (RSGs) in the H-R diagram was poorly matched by stellar evolutionary tracks (Massey 2003), with evolutionary theory failing to produce stars as cool and luminous as those “observed.” Many possible explanations might contribute to this discrepancy: there is poor knowledge of RSG molecular opacities,

the near-sonic velocities of the convective layers invalidate simplifications of mixing length theory, and the highly extended atmospheres of these stars differ from the plane-parallel geometry assumption adopted by evolutionary models. In truth, the disagreement between theory and observation lay not in deficiencies of theory, but in an incorrect placement of RSGs in the H-R diagram. Levesque et al. (2005, hereafter Paper I) used the new generation of MARCS atmosphere models (Gustafsson et al. 1975, Plez et al. 1992, Plez 2003, Gustafsson et al. 2003) to fit moderate-resolution optical spectrophotometry of 74 Galactic RSGs. The newly derived physical parameters were in excellent agreement with the Geneva evolutionary tracks for solar metallicity (Meynet & Maeder 2003).

A similar problem is known to exist for RSGs in the Magellanic Clouds (MCs), as shown in Fig. 1, where the data are from Massey & Olsen (2003), and is based upon the best available calibration at the time. One can see that the evolutionary tracks do not extend to cool enough temperatures to reproduce the “observed” (assumed) location in the H-R diagram. In addition, there is a long-standing mystery as to why the distribution of RSG spectral subtypes in the MCs is skewed towards earlier types in the MCs (Elias et al. 1985), with the average RSG being K5-K7 in the SMC, M1 in the LMC, and M2 in the Milky Way (Massey & Olsen 2003). The spectral subtype of late K- and M-type stars is largely determined on the basis of the strengths of the TiO bands, which are highly sensitive to temperature, but their strengths will obviously also depend upon the chemical abundances. Massey & Olsen (2003) proposed that the change in the distribution of spectral types was due to the lower abundances found in the Clouds ($Z/Z_{\odot} = 0.2$ for the SMC, and $Z/Z_{\odot} = 0.5$ for the LMC; see Westerlund 1997 and discussion in Massey et al. 2004); i.e., that a 3800 K star would simply appear to be of earlier spectral type in the SMC because of the lower abundance of TiO. Alternatively, as suggested by Elias et al. (1985), it is possible that stars evolve to cooler temperatures at higher metallicities than at lower, since the “Hayashi limit” (the maximum radius as a function of mass) decreases with metallicity (Hayashi & Hōshi 1961; see also Sugimoto & Nomoto 1974).

Understanding the physical properties of red supergiants at the low metallicities that characterize the Magellanic Clouds is of particular importance. Such data can be combined with that of other galaxies in the Local Group for a sensitive test of stellar evolutionary models as a function of metallicity. Observationally, the relative number of RSGs and Wolf-Rayet stars appear to change by a factor of >100 over 0.8 dex in metallicity (Massey 2002, 2003), in accordance with the suggestion first made by Maeder et al. (1980). In addition, the number ratio of RSGs to blue supergiants will be much higher at low metallicities (van den Bergh 1973), although there are challenges in determining this ratio quantitatively (Massey 2002). In the Milky Way, RSGs contribute only a few percent to the dust content of the interstellar medium, but in starburst galaxies, or galaxies at large look-back times, we expect

that RSGs will play a major role (Massey et al. 2005a), as such galaxies are usually metal-poor. Finally, the MCs represent a relatively “clean” environment, with minimal and uniform reddenings, which avoid some of the difficulties inherent in studying RSGs in the Milky Way (Paper I).

Oestreicher & Schmidt-Kaler (1998, 1999) used an earlier version of the MARCS models (Bessell et al. 1998) with their own spectrophotometry and CCD photometry to analyze a large sample of LMC stars. They conclude that the MARCS models did the best of the then-available models at fitting the data, and derived physical properties using these fits. Our work here was partially inspired by this work, and offers the following improvements. First, the MARCS models used here (and in Paper I) have been substantially revised. These now include sphericity, with an order of magnitude increase in the number of opacity sampling points, incorporate improved atomic opacities (both line and continuum), and also include improved molecular opacities (e.g., CN, CH). Second, there is now improved broad-band photometry available for *both* the LMC and SMC thanks to 2MASS and the recent CCD survey of Massey (2002). Also, our sample consists of stars whose radial velocities have been shown to be consistent with membership in the Magellanic Clouds by Massey & Olsen (2003). This list extends to stars which have cooler effective temperatures than do any of the Oestreicher & Schmidt-Kaler (1998, 1999) LMC stars. In addition, our sample includes SMC RSGs, providing important tests at even lower metallicities. Since we use the same techniques, quality of data, and modeling for RSGs in all three galaxies, differences in the derived physical properties are likely to reflect real differences, and not just methodology.

Here we present moderate-resolution spectrophotometry of 36 LMC RSGs and 39 SMC RSGs (§ 2). From these data we determine spectral types (§ 3.1), and derive physical parameters of RSGs in each of the Clouds (§ 3). As a test of the consistency of the MARCS models, we compare these to what we would derive purely on the basis of $(V - K)_0$ and $(V - R)_0$ colors (§ 3.3). In § 4 we discuss our results: we compare the extinction found for our stars to that of OB stars in the Clouds (§ 4.1), compare the newly derived physical properties to those predicted by stellar evolution theory (§ 4.2), and compare the effective temperature scales for the Magellanic Cloud RSGs to that of the Milky Way (§ 4.3). In § 5 we summarize our results, and lay out the directions for our future work.

2. Observations and Reductions

2.1. Target Selection

Our stars are listed in Table 1. The sample is drawn from Massey & Olsen (2003), who relied upon radial velocities to distinguish foreground dwarfs from MC RSGs. We expect that contamination by red giants in the halo (which would occupy a similar color and magnitude range) will be low, only a few percent, but such stars would be hard to distinguish from MC supergiants, as most of the radial velocity of the Clouds is simply due to the reflex motion of the sun. The optical photometry and positions come from Massey (2002), while the K_S values are from the Two Micron All Sky Survey (2MASS) database. The preliminary spectral types assigned by Massey & Olsen (2003) were used to ensure that a good range of spectral subtypes were observed in each Cloud. Some additional stars were observed in each Cloud, but lacked complete spectral coverage, and these stars will be discussed separately once complete data are acquired. In addition, we observed a few Galactic RSGs from Paper I to use in classifying the Magellanic Cloud stars, and to act as a check on our fluxes; this later turned out to be valuable, as detailed below.

2.2. Observations

We obtained spectroscopic data with the R-C Spectrograph on the CTIO Blanco 4-meter telescope during six nights (UT 2004 November 23-25, 1-2 Dec, 4 Dec), using the Blue Air Schmidt camera and Loral 3K CCD. We used a slit width of $375\ \mu\text{m}$ ($2.5''$), which projected to roughly 3.8 pixels on the detector. In the blue we used a $632\ \text{l mm}^{-1}$ grating (“KPGL1”) blazed at 4200\AA for coverage from 3550\AA - 6420\AA in first order at $1.01\ \text{\AA pixel}^{-1}$, with a GG-345 blocking filter to block any second-order light. In the red we used a $632\ \text{l mm}^{-1}$ grating (“KPGLF”) blazed at 8400\AA for coverage 6130\AA - 9100\AA in first order at $1.04\ \text{\AA pixel}^{-1}$, with a GG-495 blocking filter to block any second-order light. The spectral resolution was $3.8\ \text{\AA}$ for both setups. Observations in the blue were obtained on four nights (23-25 Nov 2004, 2 Dec 2004), and observations in the red on two nights (1, 4 Dec 2004). The chip was binned by 2 pixels in the spatial direction, resulting in a scale of $1.0\ \text{arcsec pixel}^{-1}$. All observations were made with the slit oriented near the parallactic angle. Conditions ranged from moderate cirrus to clear during the run, with seeing of 1.2-2.0 arcsec. Typical exposure times were 300 s in the blue, and 200 s in the red.

Bias frames were obtained each evening after the dewar was filled. Flat field calibration was obtained by taking projector flats at the beginning of each night; dome flats yielded similar solutions. Wavelength calibration was obtained by taking exposures of a He-Ne-Ar

calibration source throughout the night. Observations of spectrophotometric standards were made throughout the night, and we also included in our program several Galactic spectral standards, in common with our Galactic program (Paper I).

2.3. Reductions

We reduced the data using Image Reduction and Analysis Facility (IRAF)¹. Each frame was corrected for the bias level by a value determined from the overscan region, and then corrected for the (negligible) two-dimensional bias structure determined from average bias exposures for each night. A low-order function was fit in the dispersion direction to normalize the average of the flat-field exposures, and the normalized flat was then divided into each frame on a nightly basis. The spectra were extracted using an optimal extraction algorithm, and then wavelength corrected.

The spectrophotometric standards were used to construct sensitivity curves for each night. A grey-shift of each standard was allowed, and typically resulted in an RMS of 0.01-0.02 mag for the six or seven standard observations made each night. The standards bracketed the range of airmasses for which the program objects were observed, and standard values were assumed for the extinction.

As noted above, we observed a few Galactic RSGs from Paper I to act as spectral standards, and to serve as a consistency check on our data. Given the good agreement of the spectrophotometric standard star observations, we were quite surprised to find that several of the Galactic RSGs differed quite significantly in the near ultra-violet (NUV) fluxes, particularly below 3800Å, from what we had found in Paper I. The spectrophotometric standards agreed very well in this region, and yet the same disagreement was seen when comparing the new data to those obtained on either the Kitt Peak 2.1-m or CTIO 1.5-m telescopes (Paper I). We finally determined that the problem was inherent to the data, and not the reduction techniques. The new data all had extra flux in the NUV. We eventually noticed a strong correlation with color: the reddest red supergiants had the largest discrepancy. We also found that there was unexpected structure to the NUV flux, and in particular that there was a feature at 3810Å which looked remarkably like the telluric A-band at 7620Å, i.e., at exactly twice the wavelength of the NUV feature. The conclusion was obvious: somehow the flux at a given wavelength was being affected by the flux at twice the wavelength². Of

¹IRAF is distributed by NOAO, which is operated by AURA, Inc., under cooperative agreement with the NSF.

²We are indebted to a colleague who, upon hearing of this problem, dubbed it “the old red-leak gotcha”.

course, since we had been observing with a first-order grating in the blue, this is not the sort of typical order-separation problem that come with the lack or misuse of blocking filters. By subtracting our spectrophotometry obtained in Paper I from the current data, and comparing that to the counts in the red, we established that there was a few percent ghost of 2λ light contaminating our observations. The problem does not show up with stars of normal colors (such as that of the spectrophotometric standards), but becomes significant for the extremely red stars we observed. Tests by K.A.G.O. and P.M. in March 2005 using the comparison arcs and various blocking filters established beyond any doubt that this 632 l mm^{-1} grating also acts as a 316 l mm^{-1} grating, albeit at a low level. Another replica of this grating has been in use for many years with the Kitt Peak 4-m RC spectrograph (“KPC-007”). After our discovery, Di Harmer kindly conducted a similar test with it, and found that it suffers from the same problem.

We determined an empirical correction factor, which amounted to several percent of the 2λ count-rate, and applied that to all of our data. The spectrophotometric standards yielded the identical solutions. The correction is significant (greater than a few percent) only below 4000\AA . So as to not compromise the results of the present study, we restrict ourselves only to data long-wards of 4100\AA .

3. Analysis

3.1. Spectral Types

Since RSGs can vary in spectral type, and since our current spectra have higher signal-to-noise than those of Massey & Olsen (2003), we chose to reclassify all of the Magellanic Cloud stars in our sample. This reclassification was based primarily on the TiO band depths, which are visible even for the early and mid Ks (specifically the $\lambda 5167$ and $\lambda 6158$ TiO lines; see also Jaschek & Jaschek 1987). We strove for consistency between the classifications used here and in Paper I. The revised spectral types are compared to the older ones in Table 1.

3.2. Modeling the Spectrophotometry

Our fitting of the spectrophotometry determines three properties of these stars: effective temperature T_{eff} , the visual extinction A_V , and (indirectly) the surface gravity g [cgs]. To accomplish this, we compared our observed spectral energy distribution to a series of MARCS stellar atmosphere models. The models were computed for a metallicity $Z/Z_{\odot} = 0.2$ (SMC), and $Z/Z_{\odot} = 0.5$ (LMC). Of course, the assumption that the abundances of all elements scale

with a single “metallicity” value is a simplification, but may be a good approximation: see, for example Pritzl et al. (2005), who find that solar-like ratios of alpha-products to Fe are common even in very metal-poor systems. In any event, this serves as a useful starting point for determining the effect that chemical abundances have on the physical parameters of these stars. The models ranged from 3000 K to 4500 K in increments of 100 K and with $\log g$ values from -1 to +1, in increments of 0.5 dex. We interpolated the models for intermediate temperatures at 25 K increments. When making the fits, we reddened the models using a Cardelli et al. (1989) reddening law with $R_V = 3.1$. Although a high value of the *effective* ratio of selective-to-total extinction is needed to correct broad-band photometry of such red stars, the same R_V that works for early-type stars will work for RSGs when dealing with optical spectrophotometry; see Massey et al. (2005a).

None of the spectral features have an obvious surface gravity dependence, and so we used the same procedure as in Paper I to arrive at a final set of values. We began the fitting procedure with the $\log g = 0.0$ models, and determined the reddening and effective temperatures that gave the best fit (by eye) both to the spectral features and to the continuum. These fits were unique and well-determined, with a precision of 50 K for the M stars and the mid-to-late K stars. For the earlier K stars, our fits were based primarily on TiO $\lambda 5167$ and the G-band; we estimate that the effective temperatures of these stars have been obtained to a precision of 100 K. The extinction values A_V are determined to 0.15 mag. We next checked to see if the initial $\log g = 0.0$ value was appropriate to that expected for the star: the bolometric corrections (from the models) were used with the reddening and photometry (Table 1) to compute the bolometric luminosity, assuming true distance moduli of 18.9 (SMC) or 18.5 (LMC). The bolometric luminosity and effective temperature define an effective radius, which is used with an estimate of the mass (from a simple mass-luminosity relation determined from the Geneva evolutionary models, and which remains valid at these lower metallicities) to determine the physical $\log g$. If these $\log g$ values were closer to +0.5 or -0.5 than to our initial estimate of 0, then the star was refit with a model with a more appropriate value for the surface gravity. The calculation was then repeated, although the results converged quickly. In practice a difference in the $\log g$ value had no effect on the effective temperature, but slightly changed the extinction estimate. See Paper I for more details. We show four sample fits in Fig. 2. The complete set is available in the on-line edition, and we are also making our spectra and the models available through the Centre de Données Astronomiques de Strasbourg’s VizieR server³.

³The opacity-sampled synthetic spectra need to be smoothed in order to compare them to data. For the broad molecular bands the exact smoothing is unimportant, but for comparing atomic lines the degree of smoothing matters. For example, the slight differences between the observed spectra and fitted models

We give our final values in Table 2. In determining the bolometric luminosity we used the models to compute the bolometric correction at V as a function of effective temperature for each galaxy.

Milky Way:

$$BC_V = -298.954 + 217.532(T_{\text{eff}}/1000 \text{ K}) - 53.1400(T_{\text{eff}}/1000 \text{ K})^2 + 4.34602(T_{\text{eff}}/1000 \text{ K})^3$$

LMC:

$$BC_V = -121.364 + 78.41064(T_{\text{eff}}/1000 \text{ K}) - 16.8979(T_{\text{eff}}/1000 \text{ K})^2 + 1.20674(T_{\text{eff}}/1000 \text{ K})^3$$

SMC:

$$BC_V = -120.102 + 82.3070(T_{\text{eff}}/1000 \text{ K}) - 19.0865(T_{\text{eff}}/1000 \text{ K})^2 + 1.48927(T_{\text{eff}}/1000 \text{ K})^3$$

3.3. Analysis of Broad-Band Photometry

Although we expect that the TiO molecular band strengths will be directly affected by the abundances, and hence that the calibration of effective temperature with spectral type will depend upon metallicity, it is less clear *a priori* how the calibration of effective temperature with broad-band photometry will depend upon the metallicity. Josselin et al. (2000) have emphasized the usefulness of $(V - K)_0$ as a temperature indicator for Galactic RSGs, and in Paper I we showed that reasonable agreement exists between the physical parameters derived from fitting the spectrophotometry with those derived from $(V - K)_0$. In the optical, $(V - R)_0$ is known to be a good temperature indicator, while $(B - V)_0$ is instead dominated by surface gravity effects (Massey 1998) due to line-blanketing by weak metal lines.

3.3.1. Temperatures and Luminosities from $(V - K)_0$

In Fig. 3(a) we show the fits derived from the synthetic $(V - K)_0$ colors, derived from our models using the procedure and assumptions of Bessell et al. (1998). As in Paper I, the V

visible near 5200Å in Fig. 2 is likely due to the presence of the Mg I triplet (only partially resolved at our spectral resolution) superimposed on the TiO λ5167. Decreasing the smoothing removes most of this slight discrepancy, but introduces other problems due to the finite sampling in producing the synthetic spectra. Since this region was not used in fitting the models to the data, the disagreement in this region is cosmetic, and not indicative of a problem. We are indebted to the anonymous referee for raising this issue.

bandpass comes from Bessell (1990), while the K bandpass comes from Bessell & Brett (1988). Solar metallicity is shown in black, with the LMC metallicity indicated by red, and the SMC by green. The dispersion at each temperature is due to the range of $\log g$. The three curves show the fit to all of the data for each galaxy ($T_{\text{eff}}=3200\text{--}4300$ K, $\log g = -1, -0.5, 0, +0.5$, and $+1.0$, when available). For simplicity we have indicated the $\log g = 0.0$ models, which are the most typical of our sample, with filled circles. The dispersion with $\log g$ clearly increases with decreasing temperature, but is small for $(V - K)_0 \leq 4.5$ or $T_{\text{eff}} \geq 3600$ K. In this regime there is also little difference between the calibrations at different metallicities, with about a 30 K change (SMC minus Milky Way). The coolest stars in our Magellanic Cloud sample have $T_{\text{eff}} \sim 3475$, corresponding to $(V - K)_0 \sim 5.0$, for which the differences are -50 K (SMC minus Milky Way). The formal fits are given here:

Milky Way:

$$T_{\text{eff}} = 7741.9 - 1831.83(V - K)_0 + 263.135(V - K)_0^2 - 13.1943(V - K)_0^3$$

LMC:

$$T_{\text{eff}} = 7621.1 - 1737.74(V - K)_0 + 241.762(V - K)_0^2 - 11.8433(V - K)_0^3$$

SMC:

$$T_{\text{eff}} = 7167.5 - 1374.20(V - K)_0 + 157.000(V - K)_0^2 - 6.0481(V - K)_0^3$$

The RMS of these fits are 11 K (Galactic), 17 K (LMC), and 36 K (SMC), due primarily to the spread of $\log g$. However, in practice none of the stars in our LMC and SMC samples have extreme $\log g$ values, and as Fig. 3(a) shows, there is good agreement between our fits and the (usual) $\log g = 0.0$ case indicated by the filled circles.

How does the sensitivity of T_{eff} to color compare to the sensitivity of spectral fitting? As discussed above, we felt that the typical error for our mid-K to M stars was about 50 K. A reasonable error for $(V - K)_0$ might be 0.10 mag, given the need to correct for reddening, and we note that at 3800 K this change in color would correspond to about 35 K, smaller but comparable to the uncertainty in our spectral fitting.

Few of our Magellanic Cloud sample have “standard” K-band photometry, but all have been observed by the Two Micron All Sky Survey (2MASS) in their K_S system (i.e., the $V - K_S$ values in Table 1). Paper I cautioned that the two are not quite equivalent, and we have compared the “standard CIT” K-band photometry of Elias et al. (1985) with the K_S photometry found in the 2MASS catalog. Indeed, there is a small but non-negligible

offset, with $K_{\text{CIT}} - K_S = +0.04$. This value comes from 41 SMC stars, and has a small scatter (RMS of 0.06 mag); it is similar to the conversion found by Carpenter (2001), who find $K_{\text{CIT}} - K_S = +0.024$. Bessell & Brett (1988) find that the transformation between their adopted K bandpass (upon which our synthetic colors are based), and that of the CIT system, amounts to a constant offset $K = K_{\text{CIT}} + 0.02$. We expect therefore that $K = K_S + 0.06$ for our data-set. This is in accordance with the transformation given by Carpenter (2001), who finds that $K = K_S + 0.044$ for 2MASS data. We have corrected the $V - K_S$ values appropriately before applying the above conversion to T_{eff} . This correction is small, amounting to 20 K at $(V - K)_0 = 4.0$.

In Paper I we assumed that the extinction correction at K was $0.11A_V$ following Schlegel et al. (1998). Massey et al. (2005a) have (re)emphasized the need to carefully consider the spectral energy distribution of the source when correcting broad-band photometry of RSGs (see McCall 2004 for discussion of the general case). We have re-examined the issue here for K_S using the MARCS models and a Cardelli et al. (1989) reddening law, and find that over the range of temperatures relevant here we derive a numerical value in excellent agreement, $A_{K_S} = 0.12A_V$. Thus we expect $(V - K_S)_0 = (V - K_S) - 0.88A_V$, where the A_V values come from Table 2.

In Paper I we found that the bolometric correction at K for Galactic stars was linear with respect to effective temperature, with a small dispersion:

Milky Way:

$$BC_K = 5.574 - 0.7589(T_{\text{eff}}/1000 \text{ K}).$$

Here we find similar results for the LMC and SMC metallicities:

LMC:

$$BC_K = 5.502 - 0.7392(T_{\text{eff}}/1000 \text{ K})$$

SMC:

$$BC_K = 5.369 - 0.7029(T_{\text{eff}}/1000 \text{ K})$$

In all cases the data have been fit over the range 3200-4300 K and for $\log g = -1$ to $+1$. The dispersion is 0.01 for the Galactic and LMC metallicity models, and 0.02 mag for the SMC, where again the dispersion is mostly due to the effects of extreme surface gravities ($+1$, -1) at low effective temperatures. We show the fits in Fig. 3(b).

We list the derived effective temperatures in Table 3, and compare these to those derived from fitting the spectrophotometry in Fig. 4(a). There is clearly a systematic difference, with the $(V - K)_0$ relation predicting a higher effective temperature than the spectral fitting. We

saw a similar effect with the Galactic stars in Paper I (their Fig. 5a), although the scatter was significant, due presumably to the large (and in some cases, uncertain) reddening. Here the stars are lightly reddened, and the offset more obvious. Nevertheless, the median difference for the Galactic sample (in the sense of spectral optical minus IR) is the same as for the LMC data here, -105 K. The median difference for the SMC stars is -170 K.

This temperature difference will of course translate into a difference in the bolometric luminosities for these stars, as the bolometric correction is a steep function of effective temperature. We list the derived luminosities in Table 3, and show the comparison with those derived from fitting the spectrophotometry in Fig. 4(b). The differences amount to about -0.20 mag at the metallicity of the SMC.

This suggests that there is an inconsistency in the IR fluxes predicted by the models for a given TiO band depth. The difference amount to about 0.5 mag at K at low metallicities ($Z/Z_{\odot} = 0.2$), with better agreement at higher metallicities. What could be the cause? Josselin & Plez (2005) showed that low excitation IR CO lines in the K band computed using MARCS models are too faint compared to observations of Betelgeuse. Also, Alvarez et al. (2000), point out that their CO index is larger in RSG than in other late-type giants. However, this CO absorption not accounted for by the models cannot be responsible for the difference of 40% in the K flux we find here, and seems to exclude an unknown opacity source in the K band. Rather, the explanation might lie in the shortcomings of 1D static models. It was shown recently (Ryde et al. 2005) that MARCS models at the canonical $T_{\text{eff}} = 3600$ K for Betelgeuse cannot reproduce the IR H₂O lines around $12\mu\text{m}$, while spectra generated with a $T_{\text{eff}} = 3250$ K do reproduce the observations. In the optical a temperature of 3600 K is more appropriate. Radiative-hydrodynamical 3D models of RSG do show a pattern of large warm and cool patches on the surface (Freytag et al. 2002) that may explain this wavelength dependent T_{eff} . We can readily provide a rough estimate, at the SMC metallicity, of the impact on $(V - K)_0$ of an optical spectrum characterized by a $T_{\text{eff}} = 3600$ K ($(V - K)_0 = 4.49$) and an IR spectrum characteristic of a lower $T_{\text{eff}} = 3200$ K ($(V - K)_0 = 6.56$). Using two MARCS models at these T_{eff} and taking their V and K magnitudes, we find a composite $(V - K)_0 = 4.24$, which corresponds to a MARCS model at 3703 K. Thus, using the $(V - K)_0$ would lead to a $T_{\text{eff}} = 3700$ K, while the fitting of TiO bands would lead to $T_{\text{eff}} = 3600$ K. This explains a large part of the effect we observe, and would also impact the bolometric correction, but more detailed calculations are necessary with 3D models, or at least with patches of 1D models.

3.3.2. Temperatures and Luminosities from $(V - R)_0$

Of the optical colors, $(V - R)_0$ has the greatest potential for being used for a temperature indicator; see discussion in Massey (1998). By comparing the temperatures arrived at by $(V - R)_0$ we may also obtain useful clues as to the source of the discrepancy we found when comparing the effective temperatures derived from $(V - K)_0$ (§ 3.3.2) with those found from fitting the optical spectrophotometry (§ 3.2).

Using the Bessell (1990) approximation for the (Johnson) V and (Cousins) R filters, we have computed the expected colors for each of the MARCS models. The following fits have been made discarding the stars of extreme surface gravities ($\log g = +1, -1$):

Galactic:

$$T_{\text{eff}} = 8304.4 - 9158.6(V - R)_0 + 5675.2(V - R)_0^2 - 1194.90(V - R)_0^3$$

LMC:

$$T_{\text{eff}} = 7798.3 - 7824.4(V - R)_0 + 4554.8(V - R)_0^2 - 905.21(V - R)_0^3$$

SMC:

$$T_{\text{eff}} = 7179.4 - 6030.8(V - R)_0 + 3028.2(V - R)_0^2 - 525.98(V - R)_0^3$$

where the dispersions are 35 K, 40 K, and 68 K, respectively. We emphasize that these fits only apply to the range $T_{\text{eff}} > 3200\text{K}$, which corresponds roughly to $(V - R)_0 < 1.8$ for the Milky Way and LMC, and $(V - R)_0 < 1.5$ for the SMC. The fits are shown in Fig. 5. The sensitivity is less than that with $(V - K)_0$, as might be expected given the smaller baseline. An error of 0.05 mag in $(V - R)_0$ is not unreasonable, and would amount to an error of 90 K. The derived relationship for the LMC can be compared to that found by Oestricher & Schmidt-Kaler (1999) from the older models; the scatter from their fitting is twice as great. The temperatures agree for the warmer RSGs (50 K difference at $(V - K)_0 = 1.0$) but disagree considerably for the coolest RSGs (200 K difference at $(V - K)_0 = 1.5$).

According to Schlegel et al. (1998), we can expect that $A_R = 0.81A_V$ for the CTIO R filters, Convolution of the filter response with the MARCS models and a Cardelli et al. (1989) reddening law confirms that this is a reasonable approximation even for these very red stars, with coefficients of 0.75 (3400 K) to 0.82 (4300 K). We adopt 0.81, which is typical of our median temperatures. We list the dereddened $(V - R)_0$ colors in Table 3, along with the derived temperatures and bolometric luminosities. For the latter we assume the same A_V as

for the model fitting (i.e., Table 2), but with the BCs derived from the $(V - R)_0$ effective temperatures.

In Fig. 6(a) we show the comparison between the temperatures we derive from this method compared to those from fitting the optical spectrophotometry. We see that there is very little difference. There is a slight offset in effective temperature compared to fitting the optical spectrophotometry (-30 K for both the LMC and SMC), much less worrisome than the -105 K and -170 K found from the $(V - K)_0$ fitting. In Fig 6(b) we show the comparison between the bolometric luminosities. These agree extremely well, as expected, given the only slight offset in T_{eff} . We are forced to conclude that there is nothing wrong with our basic analysis technique, and that at present $(V - K)_0$ gives slightly inconsistent answers, probably due to the limitations of static 1D models.

4. Results

4.1. Reddening

Paper I noted that many of the RSGs in Galactic OB associations show significantly higher reddening than the early-type stars in the same clusters and associations; this matter was investigated more fully by Massey et al. (2005a), who demonstrated that this extra reddening was likely due to circumstellar dust, and amounted to as much as 4-5 mag of extra extinction at V for stars with the highest dust mass-loss rates and highest bolometric luminosities. This was in accord with a simple calculation of how much extinction one would *expect* just given the observed dust mass-loss rates and reasonable assumptions. The criticism is easily leveled that of course the Galactic OB associations suffer from variable reddenings, and that such evidence is therefore somewhat dependent upon the sample selection. We vowed to reexamine this issue in the Magellanic Clouds, where the extinction is generally low, and uniform (Massey et al. 1995, van den Bergh 2000). Of course, the lower metallicities of the Clouds should result in lower dust mass-loss rates. We hope to measure the dust mass-loss rates ourselves using the *Spitzer Space Telescope (SST)*, but even if this rate scales linearly with metallicity, we would expect to see RSGs with a considerable amount of extra extinction in the Clouds.

In Fig. 7 we compare the A_V values found from our model fitting of RSGs to the distribution of reddenings for OB stars found by Massey et al. (1995). Clearly the excess reddening we expected to find is in fact present. The peaks are shifted by several tenths of a magnitude to higher values, and there are a significant number of stars with substantially more reddening than that.

4.2. The H-R Diagram

With the improvements to the effective temperature scale given in Paper I, we found excellent agreement between the placement of RSGs in the H-R diagram and the locations of the stellar evolutionary tracks from the Geneva group (i.e., Meynet & Maeder 2003). These tracks included new opacities, and spanned a range of initial rotational velocities (0-300 km s⁻¹).

In Fig. 8(a) and (b) we make a similar comparison now using the results from fitting the optical spectrophotometry (i.e., Table 2). “Modern” models (including rotation and the revised opacities) are available at present only for higher masses for the LMC (Meynet & Maeder 2005), but a full set for the SMC is available (Maeder & Meynet 2002). We complement these with the older Geneva models, as shown in green (Schaerer et al. 1993 for the LMC and Charbonnel et al. 1993 for the SMC). We see that for the LMC there is now excellent agreement between the tracks and the “observed” (revised) locations of RSGs in the H-R diagram. For the SMC the agreement is poorer. First, the newer tracks do not extend to quite as low effective temperatures as do the data, although we note that the older tracks (shown in green) do. Still, this discrepancy is small compared to the past (Fig. 1).

More interesting is the large spread in effective temperatures of RSGs of a given luminosity in the SMC compared to that in the LMC. This effect is just what is expected: Maeder & Meynet (2001) found that, in part because massive stars formed at low metallicity have relatively weak stellar winds, little angular momentum is removed and hence rotational mixing is of increased importance at low metallicities. In this case, the helium content of red supergiants depends strongly on the rotational velocities during the main-sequence phase, and at higher helium content the tracks stop at warmer temperatures.

We can compare these two H-R diagrams to what would be obtained if instead we relied upon the $(V-K)_0$ calibration. As discussed above (§ 3.3.1) the $(V-K)_0$ calibration produces somewhat warmer temperatures than does the fitting of the optical spectrophotometry or those calculated from the broad-band $(V-R)_0$ colors. The results are similar, as shown in Fig. 8(c) and (d). No matter which calibration is used, the agreement with the evolutionary tracks is satisfactory, and is a vast improvement over the situation shown in Fig. 1. And, in either case the dispersion for the SMC is considerably greater than that for the LMC.

4.3. Effective Temperatures Scales, the Hayashi Limit, and the Distributions of Spectral Subtypes

The new effective temperature scales are compared in Table 4, and are shown in Fig. 9. For the K supergiants, the scales agree to within the errors. For cooler stars, the effective temperature scale is about 50 K cooler for LMC M-type supergiants than Galactic M-type supergiants. It is about 150 K cooler for SMC M-type supergiants than Galactic M-type supergiants.

What we find is that while an M2 I star in the Milky Way will have $T_{\text{eff}}=3660$ K, a star of similar effective temperature in the LMC would be spectroscopically identified as an M1.5 I, i.e., half a type earlier, purely due to the effect that metallicity has on the depth of the TiO bands. A star with the same effective temperature in the SMC would be spectroscopically identified as an M0 I, i.e., two spectral subtypes earlier than in the Milky Way.

This offers a partial, but incomplete, explanation for the shift in spectral subtypes first found by Elias et al. (1985), and confirmed by the more complete data of Massey & Olsen (2003). Massey & Olsen (2003) found that the average spectral type of a RSG is M2 I in the Milky Way, M1 I in the LMC, and K5-K7 I in the SMC. The spectral classifications given here are based upon better data, but the sample may be somewhat skewed towards later types. We find (from Table 4) that the average spectral type of stars in our sample is M2 I (Milky Way), M1.5 I (LMC) and K3 I (SMC). Thus, the change in the spectral appearance due to the change in abundance of TiO might be enough to explain the small shift in spectral type from the Milky Way to the LMC, but it is *not* enough to explain the relative lack of red supergiants in the SMC. Instead, we must look to the stellar evolutionary tracks.

Fig. 10 compares the evolutionary tracks for $z = 0.02$ (Milky Way, shown in black), $z = 0.008$ (LMC, shown in red), and $z = 0.004$ (SMC, shown in green). We see that there is a clear shift of the coolest tip of the tracks to warmer effective temperatures as the metallicity decreases. Elias et al. (1985) in fact attribute the shift of spectral subtypes to the effects of metallicity on the location of the red supergiant locus in the H-R diagram. The Hayashi limit denotes the largest radius a star of a given mass can have and still be in hydrodynamic equilibrium (Hayashi & Hōshi 1961⁴). This line is nearly vertical in the H-R diagram, and shifts to warmer effective temperatures at lower metallicities; we see the underlying physics reflected in the location of the coolest extent of the evolutionary tracks. Consistent with our results above (§ 4.2), this shift *is* in accordance with what we need to explain the change

⁴Sugimoto & Nomoto (1974) present a nice heuristic derivation based upon the argument that the average density of a star must be greater than its photospheric density.

in spectral subtype. For a 15-25 M_{\odot} star we expect a shift in effective temperatures of red supergiants of about +500 K from Milky Way (black) to SMC (green). This is actually larger than the required shift, about 350 K (Table 4). From the Milky Way to the LMC the tracks shift by 100 to 150 K, in good agreement with the shift in average spectral type from M2 (Milky Way) to M1-M1.5 (LMC). Thus we conclude that the shift in the spectral type due to the abundance of TiO is a secondary effect, and that the main reason that the spectral subtypes are earlier in the Clouds than in the Milky Way is due to the shift of the Hayashi limit with metallicity. This is in accordance with the speculation offered by Elias et al. (1985).

5. Summary and Conclusions

We have derived new physical properties of RSGs in the Magellanic Clouds, using the MARCS stellar atmosphere models, following our treatment of Galactic RSGs in Paper I. We find that the effective temperatures of K supergiants are about the same in the SMC, LMC, and Milky Way, but that the lower abundance of TiO leads to effective temperatures that are about 50 K lower (LMC) and 150 K lower for M supergiants of the same spectral subtype. To put this in a more physical way, a star in the same place in the H-R diagram that is called an M2 I in the Milky Way, would be of M1.5 I type in the LMC, and M0 I in the SMC. This is not sufficient to explain the shift with metallicity in the average spectral types between the Milky Way and the SMC, where the average spectral types of RSGs change from M2 I to K3 I. Instead, it is primarily the change in the Hayashi limit with metallicity that is responsible. This agrees with the explanation offered by Elias et al. (1985), who first observed the shift in type.

Although the MARCS models give very good fits to the optical spectrophotometry, the results derived from this fitting do result in temperatures that are systematically cooler than those that would be derived from the observed $(V - K)_0$ colors. The median discrepancy is about -100 K for the Milky Way and the LMC, and -170 K for the SMC. This systematic difference is likely due to the limitations of static 1D models. The $(V - R)_0$ colors produce temperatures that are more consistent with the optical spectrophotometry, with only a small offset (-30 K) for both the SMC and the LMC.

Although we would of course prefer for all techniques to give perfect agreement, we can place this discrepancy into context. A 175 K difference in the effective temperature scale is a 4-5% effect. For comparison, recent revisions to the effective temperatures of O-type stars have shifted the scale by 10% (see discussion in Massey et al. 2005b).

The RSGs in our sample show higher extinction on average than do the OB stars in the Clouds; this is consistent with our findings that many Galactic RSGs have higher extinction than OB stars in the same clusters and associations (Paper I). Massey et al. (2005a) argue that this is a natural consequence of the fact that these stars are “smokey”, and produce circumstellar dust. Follow-up ground-based observations were successfully obtained in December 2005 to derive the extinction properties of this dust, and we hope to extend this work using the *SST*.

The newly derived properties provide an excellent match to stellar evolution tracks in the LMC, but there is significantly more scatter for the SMC. This may be due to the larger effect that rotational mixing has in lower metallicity stars (Maeder & Meynet, 2001). The helium content of red supergiants is changes significantly (typically by $\Delta Y = 0.10$ or more) as a function of the rotation velocities during the main-sequence phase. A higher helium abundance results in the evolutionary tracks stopping at slightly warmer temperatures than in the absence of such enrichment. However, the amount of helium enrichment critically depends on the assumed physics of the models. In this context, observational determinations of the He/H ratios would be very useful indeed.

Throughout this work we have made the approximation that the abundances of the SMC and LMC scale by a single number, a fact which we know is not quite correct. (For a good discussion of this see Venn 1999 and Dufour 1984.) As improved stellar models (with improved opacities and which include the effects of rotation) become available at the relevant mass range (10-20 M_{\odot}) we will better know what individual abundances to assume for the model atmospheres. In the meanwhile, we believe that the current study accurately represents the differential correction to the derived properties of RSGs. We also plan to extend this work to the metal-rich environment found in the Andromeda Galaxy.

We are grateful to Hernan Tirado and Ricardo Venegas for excellent support with the RC spectrograph, both during our observing and for the follow-up daytime tests to track down the elusive grating problem. As always, observing at CTIO was a pleasure. The preliminary part of this work was supported under NSF grant AST 00-093060; additional support was provided through the Friends of Lowell Observatory. This paper made use of data products from the 2MASS, which is a joint project of the University of Massachusetts and the Infrared Processing and Analysis Center/California Institute of Technology, funded by the National Aeronautics and Space Administration and the National Science Foundation. An anonymous referee made useful comments on the paper, leading to some substantial improvements; Deidre Hunter also kindly provided a critical reading of the manuscript.

REFERENCES

- Alvarez, R., Laçon, A., Plez, B., & Wood, P. R. 2000, *A&A*, 353, 322
- Bessell, M. S. 1990, *PASP*, 102, 1181
- Bessell, M. S. & Brett, J. M. 1988, *PASP*, 100, 1134
- Bessell, M. S., Castelli, F., & Plez, B. 1998, *A&A*, 333, 231
- Cardelli, J. A., Clayton, G. C., & Mathis, J. S. 1989, *ApJ*, 345, 245
- Carpenter, J. M. 2001, *AJ*, 121, 2851
- Charbonnel, C., Meynet, G., Maeder, A., Schaller, G., & Schaerer, D. 1993, *A&AS*, 101, 415
- Dufour, R. J. 1984, in *IAU Symp.108, Structure and Evolution of the Magellanic Clouds*, ed. S. van den Bergh & K. S. de Boer (Dordrecht: Reidel), 353
- Elias, J. H., Frogel, J. A., & Humphreys, R. M. 1985, *ApJS*, 57, 91
- Freytag, B., Steffen, M., & Dorch, B. 2002, *Astron Nach*, 323, 213
- Gustafsson, B., Bell, R. A., Eriksson, K., & Nordlund, Å 1975, *A&A*, 42, 407
- Gustafsson, B., Edvardsson, B., Eriksson, K., Mizumo-Wiedner, M., Jorgensen, U. G., & Plez, B. 2003, in *ASP Conf. Ser. 288, Stellar Atmosphere Modeling*, ed. I. Hubeny, D. Mihalas, & K. Werner (San Francisco: ASP), 331
- Hayashi, C., & Hōshi, R. 1961, *PASJ*, 13, 442
- Jaschek, C., & Jaschek, M. 1987, *The Classification of Stars* (Cambridge: Cambridge University Press)
- Josselin, E., Blommaert, J. A. D. L., Groenewegen, M. A. T., Omont, A., & Li, F. L. 2000, *A&A*, 357, 225
- Josselin, E., & Plez, B. 2005, in *High Resolution Infrared Spectroscopy in Astronomy*. ed. H.U. Käufel, R. Siebenmorgen, & A.F.M. Moorwood (Berlin: Springer), 405
- Levesque, E. M., Massey, P., Olsen, K. A. G., Plez, B., Josselin, E., Maeder, A., & Meynet, G. 2005, *ApJ*, 628, 973
- Maeder, A., Lequeux, J., & Azzopardi, M. 1980, *A&A*, 90, L17
- Maeder, A., & Meynet, G. 2000, *ARA&A*, 38, 143
- Maeder, A., & Meynet, G. 2001, *A&A*, 373, 555
- Massey, P. 1998, *ApJ*, 501, 153
- Massey, P. 2002, *ApJS*, 141, 81
- Massey, P. 2003, *ARA&A*, 41, 15

- Massey, P., Bresolin, F., Kudritzki, R. P., Puls, J., Pauldrach, A. W. A. 2004, *ApJ*, 608, 1001
- Massey, P., Lang, C. C., DeGioia-Eastwood, K., & Garmany, C. D. 1995, *ApJ*, 438, 188
- Massey, P., & Olsen, K. A. G. 2003, *AJ*, 126, 2867
- Massey, P., Plez, B., Levesque, E. M., Olsen, K. A. G., Clayton, G. C., & Josselin, E. 2005a, *ApJ*, 634, 1286
- Massey, P., Puls, J., Pauldrach, A. W. A., Bresolin, F., Kudritzki, R. P., & Simon, T. 2005b, *ApJ*, 627, 477
- Meynet, G. & Maeder, A. 2003, *A&A*, 404, 975
- Meynet, G., & Maeder, A. 2005, *A&A*, 429, 581
- Oestreich, M. O. & Schmidt-Kaler, Th. 1998, *MNRAS*, 299, 625
- Oestreich, M. O. & Schmidt-Kaler, Th. 1999, *Astron. Natur.* 320, 385
- Plez, B. 2003, in *ASP Conf. Ser.* 298, *GAI*A Spectroscopy: Science and Technology, ed. U. Munari (San Francisco: ASP), 189
- Plez, B., Brett, J. M., & Nordlund, Å 1992, *A&A*, 256, 551
- Pritzl, B. J., Venn, K. A., & Irwin, M. 2005, *AJ*, 130, 2140
- Ryde, N., Harper, G. M., Richter, M. J., Greathouse, T. K., & Lacy, J. H. 2006, *ApJ*, 637, 1040
- Schaerer, D., Meynet, G., Maeder, A., & Schaller, G. 1993, *A&AS*, 98, 523
- Schlegel, D. J., Finkbeiner, D. P., & Davis, M. 1998, *ApJ*, 500, 525
- Sugimoto, D., & Nomoto, K. 1974, in *Late Stages of Stellar Evolution*, IAU Symp. 66, ed. R. J. Tayler & J. E. Hesser (Dordrecht: Reidel), 105
- van den Bergh, S. 1973, *ApJ*, 183, L123
- van den Bergh, S. 2000, *The Galaxies of the Local Group* (Cambridge: Cambridge University Press)
- Venn, K. A. 1999, *ApJ*, 518, 405.
- Westerlund, B. E. 1997, *The Magellanic Clouds* (Cambridge: Cambridge University Press)

Table 1. Program Stars^a

Star	α_{2000}	δ_{2000}	V	$B - V$	$V - R$	$V - K_S^b$	Spectral Type	
							Old ^c	New
SMC005092	00 45 04.56	-73 05 27.4	12.90	2.03	1.18	4.83	M1 I	M2 I
SMC008930	00 47 36.94	-73 04 44.3	12.68	2.00	1.06	4.36	K7 I	M0 I
SMC010889	00 48 27.02	-73 12 12.3	12.20	2.00	1.06	4.43	K7 I	M0 I
SMC011101	00 48 31.92	-73 07 44.4	13.54	1.69	0.99	4.30	K7 I	K2.5 I
SMC011709	00 48 46.32	-73 28 20.7	12.43	1.79	0.94	3.90	K7 I	K5-M0 I
SMC011939	00 48 51.83	-73 22 39.3	12.82	1.81	1.00	4.21	M0 I	K2 I
SMC012322	00 49 00.32	-72 59 35.7	12.44	1.93	1.03	4.16	M0 I	K5-M0 I
SMC013740	00 49 30.34	-73 26 49.9	13.47	1.77	0.96	4.08	K7 I	K3 I
SMC013951	00 49 34.42	-73 14 09.9	13.00	1.79	0.93	3.94	K7 I	K3 I
SMC015510	00 50 06.42	-73 28 11.1	12.59	1.90	0.95	4.06	M0 I	K5 I
SMC018136	00 50 56.01	-72 15 05.7	11.98	1.95	1.01	4.13	M0 I	M0 I
SMC020133	00 51 29.68	-73 10 44.3	12.33	1.95	1.03	4.18	M0 I	M0 I
SMC021362	00 51 50.25	-72 05 57.2	12.89	1.86	0.95	4.07	K5-M0 I	K5 I
SMC021381	00 51 50.46	-72 11 32.2	12.81	1.81	0.92	3.81	K5-M0 I	K5 I
SMC023401	00 52 25.36	-72 25 13.3	12.99	1.71	0.84	3.56	K5 I	K1 I
SMC023743	00 52 31.49	-72 11 37.3	12.98	1.65	0.84	3.57	K5-M0 I	K2 I
SMC025879	00 53 08.87	-72 29 38.6	11.91	1.77	0.88	3.46	K7 I	M0 I
SMC030135	00 54 26.90	-72 52 59.4	12.84	1.68	0.78	3.35	K0-2 I	K2 I
SMC030616	00 54 35.90	-72 34 14.3	12.22	1.85	0.92	3.88	K7 I	K2 I
SMC034158	00 55 36.58	-72 36 23.6	12.79	1.78	0.95	3.88	K7 I	K2 I
SMC035445	00 55 58.84	-73 20 41.4	12.74	1.77	0.91	3.76	M0 I	K1 I
SMC042438	00 58 08.71	-72 19 26.7	13.20	1.59	0.87	3.84	K3-5 I	K2 I
SMC043219	00 58 23.30	-72 48 40.7	13.06	1.84	0.94	3.95	M0 I	K2 I
SMC045378	00 59 07.16	-72 13 08.6	12.93	1.56	0.92	3.93	K5 I	K3 I
SMC046497	00 59 31.33	-72 15 46.4	12.40	1.98	0.99	4.09	M1 I	K5-M0 I
SMC046662	00 59 35.04	-72 04 06.2	12.90	1.88	1.07	4.55	M2 I	K3 I
SMC048122	01 00 09.42	-72 08 44.5	12.19	1.78	0.89	3.46	K3 I	K1 I
SMC049478	01 00 41.56	-72 10 37.0	12.17	1.81	0.99	4.21	M0 I	K5-M0 I
SMC050028	01 00 55.12	-71 37 52.6	11.81	1.82	0.97	3.77	M0 I	K1 I
SMC050840	01 01 15.99	-72 13 10.0	12.57	1.95	1.02	4.20	M1-2 I	M1 I
SMC054708	01 02 51.37	-72 24 15.5	12.82	1.81	0.91	3.74	K0 I	K1 I
SMC055681	01 03 12.98	-72 09 26.5	12.52	1.65	0.96	3.93	M3 I	K5-M0 I
SMC056732	01 03 34.30	-72 06 05.8	12.86	1.53	0.94	4.00	K7 I	K5-M0 I
SMC057386	01 03 47.35	-72 01 16.0	12.71	1.57	0.85	3.74	K3-5 I	K1 I
SMC057472	01 03 48.89	-72 02 12.7	12.80	1.83	0.88	3.83	K5-7 I	K2 I
SMC059803	01 04 38.16	-72 01 27.2	11.98	1.95	0.98	3.88	M0-1 I	K2-3 I
SMC060447	01 04 53.05	-72 47 48.5	13.09	1.64	0.94	3.91	M0 I	K2 I
SMC067509	01 08 13.34	-72 00 02.9	12.74	1.68	0.86	3.57	K2 I	K1 I
SMC069886	01 09 38.08	-73 20 01.9	11.74	1.95	1.04	3.95	M2 I	K5-M0 I
LMC054365	05 02 09.57	-70 25 02.4	13.26	1.85	1.10	4.94	M3 I	M2.5 I
LMC061753	05 03 59.77	-69 38 15.0	13.16	2.07	1.16	5.14	M2 I	M2 I
LMC062090	05 04 05.10	-70 22 46.7	12.50	1.96	1.00	4.39	M1 I	M1 I
LMC064048	05 04 41.79	-70 42 37.2	13.28	1.89	1.19	5.25	M3 I	M2.5 I
LMC065558	05 05 10.03	-70 40 03.2	12.62	1.89	1.01	4.24	M0 I	M1 I
LMC067982	05 05 56.61	-70 35 24.0	12.76	1.93	1.09	4.65	M4.5 I	M2.5 I

Table 1—Continued

Star	α_{2000}	δ_{2000}	V	$B - V$	$V - R$	$V - K_S^b$	Spectral Type	
							Old ^c	New
LMC068098	05 05 58.92	-70 29 14.6	13.11	1.90	1.04	4.64	M1 I	M1.5 I
LMC068125	05 05 59.56	-70 48 11.4	13.43	1.83	1.20	5.12	M4 I	M4 I
LMC109106	05 17 56.51	-69 40 25.4	12.96	1.85	1.02	4.39	M2 I	M2.5 I
LMC116895	05 19 53.34	-69 27 33.4	12.43	1.92	1.03	4.21	M3 I	M0 I
LMC119219	05 20 23.69	-69 33 27.3	12.14	2.04	0.98	4.16	M3 I	M3 I
LMC131735	05 23 34.09	-69 19 07.0	12.65	1.84	0.89	3.75	K7 I	K2 I
LMC134383	05 25 44.95	-69 04 48.9	13.46	1.65	1.21	5.47	M3 I	M2.5 I
LMC135720	05 26 27.52	-69 10 55.5	13.57	1.85	1.35	5.86	M3 I	M4.5 I
LMC136042	05 26 34.92	-68 51 40.1	12.24	1.08	1.09	4.97	M1 I	M3 I
LMC137624	05 27 10.38	-69 16 17.6	13.16	1.88	1.02	4.38	M0 I	M0 I
LMC137818	05 27 14.33	-69 11 10.7	13.33	1.74	1.20	5.14	M3 I	M2 I
LMC138405	05 27 26.86	-69 00 02.0	13.08	1.83	1.02	4.41	M0 I	M1 I
LMC140296	05 28 06.11	-69 07 13.5	13.12	1.87	1.18	4.97	M1-2 I	M2 I
LMC141430	05 28 28.98	-68 07 07.8	12.30	2.15	1.24	4.82	M0 I ^d	M1 I
LMC142202	05 28 45.59	-68 58 02.3	12.15	1.65	1.03	4.60	M0-M1 I	M1.5 I
LMC142907	05 29 00.86	-68 46 33.6	13.05	1.89	1.06	4.61	M1 I	M2 I
LMC143877	05 29 21.10	-68 47 31.5	11.82	1.94	0.95	3.85	K7 I	K3 I
LMC146126	05 30 02.36	-67 02 45.0	11.17	1.80	0.84	3.20	K5 I	K5 I
LMC147199	05 30 21.00	-67 20 05.7	12.73	1.57	1.20	5.28	M4 I	M1.5 I
LMC149721	05 31 03.50	-69 05 40.0	12.71	1.86	0.97	4.13	K5-7 I	M0 I
LMC157533	05 33 29.67	-67 31 38.0	13.16	1.50	0.99	4.34	K5 I	K5 I
LMC158317	05 33 44.60	-67 24 16.9	13.35	1.96	1.12	4.86	M2 I	M1 I
LMC159974	05 34 21.49	-69 21 59.8	12.72	1.77	0.91	3.83	K2-5 I	K1 I
LMC169754	05 37 58.77	-69 14 23.7	13.21	2.15	1.13	4.83	K2-3 I	K2 I
LMC174714	05 40 24.48	-69 21 16.6	13.13	1.98	1.21	5.28	M4-5 I	M1.5 I
LMC175464	05 40 55.36	-69 23 25.0	12.90	2.20	1.22	5.36	M2-3 I	M2 I
LMC175746	05 41 06.94	-69 17 14.8	13.30	2.06	1.26	5.53	M3 I	M3 I
LMC176890	05 41 50.26	-69 21 15.7	12.85	1.97	1.01	4.29	K7 I	M0 I
LMC177150	05 42 00.84	-69 11 37.0	13.80	1.89	1.20	5.12	M1 I	M1.5 I
LMC177997	05 42 35.48	-69 08 48.3	12.56	2.02	1.08	4.85	M2 I ^d	M1.5 I

^aStar identification and optical photometry from Massey 2002

^b K_S photometry from 2MASS point-source catalog.

^cOld spectral type from Massey & Olsen 2003 for all stars unless otherwise noted.

^dOld spectral type from Elias et al. 1985

Table 2. Results of Spectral Fits

Star	Spectral Type	T_{eff}	A_V	$\log g$		R/R_{\odot}	M_V	M_{bol}
				Model	Actual			
SMC005092	M2 I	3475	0.40	-0.5	-0.4	1220	-6.40	-8.48
SMC008930	M0 I	3625	0.56	0.0	-0.3	1070	-6.78	-8.38
SMC010889	M0 I	3600	0.09	-0.5	-0.3	1130	-6.79	-8.47
SMC011101	K2.5 I	4200	1.43	0.0	0.2	540	-6.79	-7.55
SMC011709	K5-M0 I	3725	0.09	0.0	-0.1	830	-6.56	-7.93
SMC011939	K2 I	4025	1.05	0.0	0.0	750	-7.13	-8.05
SMC012322	K5-M0 I	3750	0.56	0.0	-0.2	980	-7.02	-8.34
SMC013740	K3 I	3750	0.34	0.0	0.2	550	-5.77	-7.09
SMC013951	K3 I	4225	1.12	0.0	0.2	590	-7.02	-7.76
SMC015510	K5 I	3850	0.68	0.0	-0.1	850	-6.99	-8.13
SMC018136	M0 I	3575	0.09	-0.5	-0.4	1310	-7.01	-8.76
SMC020133	M0 I	3625	0.22	-0.5	-0.3	1080	-6.79	-8.39
SMC021362	K5 I	3775	0.25	0.0	0.0	670	-6.26	-7.53
SMC021381	K5 I	3800	0.28	0.0	0.0	680	-6.37	-7.59
SMC023401	K1 I	4075	0.40	0.0	0.3	490	-6.31	-7.18
SMC023743	K2 I	4050	0.25	0.0	0.3	470	-6.17	-7.06
SMC025879	M0 I	3700	0.03	-0.5	-0.3	1060	-7.02	-8.44
SMC030135	K2 I	4050	0.28	0.0	0.2	510	-6.34	-7.23
SMC030616	K2 I	3850	0.40	0.0	-0.1	880	-7.08	-8.22
SMC034158	K2 I	4075	0.90	0.0	0.1	670	-7.01	-7.88
SMC035445	K1 I	4100	0.65	0.0	0.1	600	-6.81	-7.66
SMC042438	K2 I	4250	0.99	0.0	0.3	500	-6.69	-7.41
SMC043219	K2 I	3850	0.28	0.0	0.2	570	-6.12	-7.26
SMC045378	K3 I	3850	0.47	0.0	0.1	660	-6.43	-7.58
SMC046497	K5-M0 I	3700	0.37	0.0	-0.2	990	-6.87	-8.30
SMC046662	K3 I	4100	1.24	0.0	0.0	730	-7.24	-8.08
SMC048122	K1 I	4225	0.81	0.0	0.0	740	-7.52	-8.26
SMC049478	K5-M0 I	3700	0.34	0.0	-0.3	1080	-7.07	-8.49
SMC050028	K1 I	4300	1.36	0.0	-0.2	1080	-8.45	-9.14
SMC050840	M1 I	3625	0.19	0.0	-0.2	950	-6.52	-8.12
SMC054708	K1 I	4300	0.99	0.0	0.2	570	-7.07	-7.76
SMC055681	K5-M0 I	4100	1.18	0.0	-0.1	850	-7.56	-8.40
SMC056732	K5-M0 I	3725	0.25	0.0	0.0	730	-6.29	-7.66
SMC057386	K1 I	4300	0.87	0.0	0.2	570	-7.06	-7.74
SMC057472	K2 I	4100	0.65	0.0	0.2	580	-6.75	-7.60
SMC059803	K2-3 I	4100	0.93	0.0	-0.2	970	-7.85	-8.69
SMC060447	K2 I	3900	0.50	0.0	0.1	580	-6.31	-7.37
SMC067509	K1 I	4175	0.56	0.0	0.2	540	-6.72	-7.50
SMC069886	K5-M0 I	3750	0.28	-0.5	-0.3	1190	-7.44	-8.76
LMC054365	M2.5 I	3525	0.56	0.0	-0.2	900	-5.80	-7.88
LMC061753	M2 I	3600	0.68	0.0	-0.1	830	-6.02	-7.80
LMC062090	M1 I	3700	0.47	0.0	-0.1	830	-6.47	-7.92
LMC064048	M2.5 I	3500	0.40	0.0	-0.2	880	-5.62	-7.81
LMC065558	M1 I	3725	0.31	0.0	0.0	700	-6.19	-7.57
LMC067982	M2.5 I	3575	0.65	0.0	-0.3	1040	-6.39	-8.27

Table 2—Continued

Star	Spectral Type	T_{eff}	A_V	$\log g$		R/R_{\odot}	M_V	M_{bol}
				Model	Actual			
LMC068098	M1.5 I	3700	0.56	0.0	0.0	650	-5.95	-7.40
LMC068125	M4 I	3475	0.84	0.0	-0.3	1080	-5.91	-8.21
LMC109106	M2.5 I	3550	0.37	0.0	-0.2	890	-5.91	-7.89
LMC116895	M0 I	3750	0.71	0.0	-0.2	880	-6.78	-8.10
LMC119219	M3 I	3575	0.25	-0.5	-0.3	1150	-6.61	-8.48
LMC131735	K2 I	4150	0.77	0.0	0.2	510	-6.62	-7.36
LMC134383	M2.5 I	3575	0.77	0.0	-0.1	800	-5.81	-7.69
LMC135720	M4.5 I	3425	0.90	-0.5	-0.4	1200	-5.83	-8.38
LMC136042	M3 I	3500	0.09	-0.5	-0.4	1240	-6.35	-8.54
LMC137624	M0 I	3700	0.40	0.0	0.1	600	-5.74	-7.19
LMC137818	M2 I	3625	0.71	0.0	-0.1	740	-5.88	-7.57
LMC138405	M1 I	3675	0.40	0.0	0.0	650	-5.82	-7.35
LMC140296	M2 I	3625	1.15	0.0	-0.2	990	-6.53	-8.22
LMC141430	M1 I	3700	0.90	-0.5	-0.3	1110	-7.10	-8.55
LMC142202	M1.5 I	3650	0.40	-0.5	-0.3	1050	-6.75	-8.36
LMC142907	M2 I	3650	0.68	0.0	-0.1	790	-6.13	-7.74
LMC143877	K3 I	3900	0.90	0.0	-0.2	1010	-7.58	-8.58
LMC146126	K5 I	3875	0.25	0.0	-0.2	1050	-7.58	-8.62
LMC147199	M1.5 I	3675	0.53	0.0	-0.1	810	-6.30	-7.82
LMC149721	M0 I	3750	0.40	0.0	0.0	670	-6.19	-7.51
LMC157533	K5 I	3825	0.53	0.0	0.2	510	-5.87	-7.00
LMC158317	M1 I	3675	0.77	0.0	0.0	680	-5.92	-7.45
LMC159974	K1 I	4300	1.24	0.0	0.2	560	-7.02	-7.72
LMC169754	K2 I	4100	1.95	0.0	0.0	700	-7.24	-8.01
LMC174714	M1.5 I	3625	1.33	0.0	-0.3	1080	-6.70	-8.39
LMC175464	M2 I	3625	1.33	-0.5	-0.4	1200	-6.93	-8.62
LMC175746	M3 I	3550	1.18	0.0	-0.3	1100	-6.38	-8.35
LMC176890	M0 I	3750	0.56	0.0	0.0	670	-6.21	-7.52
LMC177150	M1.5 I	3600	0.77	0.0	0.0	650	-5.47	-7.26
LMC177997	M1.5 I	3675	0.77	0.0	-0.2	980	-6.71	-8.24

Table 3. Results from Broad Band Photometry

Star	Spectral Type	Spectral Fit ^a		Results from $(V - K)_0$					Results from $(V - R)_0$				
		T_{eff}	M_{bol}	$(V - K)_0^b$	T_{eff}	ΔT_{eff}^c	M_{bol}	ΔM_{bol}^d	$(V - R)_0^e$	T_{eff}	ΔT_{eff}^c	M_{bol}	ΔM_{bol}^d
SMC005092	M2 I	3475	-8.48	4.42	3639	-163	-8.01	-0.47	1.10	3504	-28	-8.37	-0.11
SMC008930	M0 I	3625	-8.38	3.81	3878	-252	-7.94	-0.44	0.95	3726	-100	-8.15	-0.23
SMC010889	M0 I	3600	-8.47	4.29	3684	-83	-8.30	-0.17	1.04	3587	13	-8.50	0.03
SMC011101	K2.5 I	4200	-7.55	2.98	4306	-105	-7.43	-0.12	0.72	4215	-14	-7.54	-0.01
SMC011709	K5-M0 I	3725	-7.93	3.76	3898	-172	-7.69	-0.24	0.92	3779	-53	-7.82	-0.11
SMC011939	K2 I	4025	-8.05	3.23	4165	-139	-7.91	-0.14	0.80	4022	3	-8.05	0.00
SMC012322	K5-M0 I	3750	-8.34	3.61	3969	-218	-8.05	-0.29	0.92	3778	-27	-8.28	-0.06
SMC013740	K3 I	3750	-7.09	3.72	3916	-165	-6.87	-0.22	0.90	3830	-79	-6.94	-0.15
SMC013951	K3 I	4225	-7.76	2.89	4359	-133	-7.61	-0.15	0.72	4218	7	-7.77	0.01
SMC015510	K5 I	3850	-8.13	3.40	4072	-221	-7.88	-0.25	0.82	3979	-128	-7.96	-0.17
SMC018136	M0 I	3575	-8.76	3.99	3799	-223	-8.30	-0.46	0.99	3662	-86	-8.52	-0.24
SMC020133	M0 I	3625	-8.39	3.93	3826	-200	-8.04	-0.35	0.99	3669	-43	-8.28	-0.11
SMC021362	K5 I	3775	-7.53	3.79	3885	-109	-7.41	-0.12	0.90	3816	-40	-7.46	-0.07
SMC021381	K5 I	3800	-7.59	3.50	4020	-219	-7.33	-0.26	0.87	3885	-84	-7.46	-0.13
SMC023401	K1 I	4075	-7.18	3.15	4209	-133	-7.05	-0.13	0.76	4105	-29	-7.15	-0.03
SMC023743	K2 I	4050	-7.06	3.29	4130	-79	-6.99	-0.07	0.79	4040	10	-7.07	0.01
SMC025879	M0 I	3700	-8.44	3.37	4086	-385	-7.90	-0.54	0.87	3870	-169	-8.13	-0.31
SMC030135	K2 I	4050	-7.23	3.04	4269	-218	-7.02	-0.21	0.73	4194	-143	-7.11	-0.12
SMC030616	K2 I	3850	-8.22	3.47	4038	-187	-8.02	-0.20	0.84	3930	-79	-8.11	-0.11
SMC034158	K2 I	4075	-7.88	3.03	4278	-202	-7.68	-0.20	0.78	4070	5	-7.88	0.00
SMC035445	K1 I	4100	-7.66	3.13	4220	-119	-7.54	-0.12	0.79	4053	47	-7.70	0.04
SMC042438	K2 I	4250	-7.41	2.91	4350	-99	-7.29	-0.12	0.68	4308	-57	-7.37	-0.04
SMC043219	K2 I	3850	-7.26	3.64	3952	-101	-7.17	-0.09	0.89	3846	4	-7.27	0.01
SMC045378	K3 I	3850	-7.58	3.46	4044	-193	-7.37	-0.21	0.83	3958	-107	-7.43	-0.15
SMC046497	K5-M0 I	3700	-8.30	3.70	3924	-223	-7.96	-0.34	0.92	3785	-84	-8.12	-0.18
SMC046662	K3 I	4100	-8.08	3.40	4073	27	-8.13	0.05	0.83	3950	150	-8.24	0.16
SMC048122	K1 I	4225	-8.26	2.69	4491	-265	-7.99	-0.27	0.74	4171	54	-8.30	0.04
SMC049478	K5-M0 I	3700	-8.49	3.85	3858	-157	-8.26	-0.23	0.93	3775	-74	-8.34	-0.15
SMC050028	K1 I	4300	-9.14	2.51	4609	-308	-8.83	-0.31	0.71	4232	68	-9.19	0.05
SMC050840	M1 I	3625	-8.12	3.97	3807	-181	-7.80	-0.32	0.98	3676	-50	-8.00	-0.12
SMC054708	K1 I	4300	-7.76	2.81	4412	-111	-7.61	-0.15	0.72	4206	94	-7.83	0.07
SMC055681	K5-M0 I	4100	-8.40	2.83	4398	-297	-8.11	-0.29	0.74	4172	-71	-8.34	-0.06
SMC056732	K5-M0 I	3725	-7.66	3.72	3917	-191	-7.39	-0.27	0.89	3835	-109	-7.46	-0.20
SMC057386	K1 I	4300	-7.74	2.91	4346	-45	-7.66	-0.08	0.68	4301	0	-7.74	0.00

Table 3—Continued

Star	Spectral Type	Spectral Fit ^a		Results from $(V - K)_0$					Results from $(V - R)_0$				
		T_{eff}	M_{bol}	$(V - K)_0^b$	T_{eff}	ΔT_{eff}^c	M_{bol}	ΔM_{bol}^d	$(V - R)_0^e$	T_{eff}	ΔT_{eff}^c	M_{bol}	ΔM_{bol}^d
SMC057472	K2 I	4100	-7.60	3.20	4181	-80	-7.52	-0.08	0.76	4122	-21	-7.58	-0.02
SMC059803	K2-3 I	4100	-8.69	3.00	4294	-193	-8.50	-0.19	0.80	4016	84	-8.78	0.09
SMC060447	K2 I	3900	-7.37	3.41	4067	-166	-7.21	-0.16	0.84	3928	-27	-7.34	-0.03
SMC067509	K1 I	4175	-7.50	3.02	4284	-108	-7.38	-0.12	0.75	4129	46	-7.54	0.04
SMC069886	K5-M0 I	3750	-8.76	3.64	3952	-201	-8.49	-0.27	0.99	3672	78	-8.93	0.17
LMC054365	M2.5 I	3525	-7.88	4.39	3651	-125	-7.38	-0.50	0.99	3633	-107	-7.46	-0.42
LMC061753	M2 I	3600	-7.80	4.48	3623	-22	-7.68	-0.12	1.03	3581	19	-7.87	0.07
LMC062090	M1 I	3700	-7.92	3.92	3812	-111	-7.70	-0.22	0.91	3767	-66	-7.74	-0.18
LMC064048	M2.5 I	3500	-7.81	4.84	3532	-31	-7.57	-0.24	1.11	3483	17	-7.88	0.07
LMC065558	M1 I	3725	-7.57	3.91	3816	-90	-7.42	-0.15	0.95	3698	27	-7.65	0.08
LMC067982	M2.5 I	3575	-8.27	4.02	3774	-198	-7.70	-0.57	0.97	3674	-98	-7.92	-0.35
LMC068098	M1.5 I	3700	-7.40	4.09	3749	-48	-7.31	-0.09	0.93	3727	-26	-7.33	-0.07
LMC068125	M4 I	3475	-8.21	4.32	3671	-195	-7.44	-0.77	1.04	3569	-93	-7.81	-0.40
LMC109106	M2.5 I	3550	-7.89	4.00	3779	-228	-7.21	-0.68	0.95	3700	-149	-7.36	-0.53
LMC116895	M0 I	3750	-8.10	3.53	3981	-230	-7.75	-0.35	0.90	3795	-44	-7.98	-0.12
LMC119219	M3 I	3575	-8.48	3.88	3826	-250	-7.82	-0.66	0.93	3729	-153	-7.98	-0.50
LMC131735	K2 I	4150	-7.36	3.01	4256	-105	-7.28	-0.08	0.74	4126	24	-7.37	0.01
LMC134383	M2.5 I	3575	-7.69	4.73	3557	18	-7.67	-0.02	1.06	3540	35	-7.83	0.14
LMC135720	M4.5 I	3425	-8.38	5.01	3494	-68	-7.92	-0.46	1.18	3421	4	-8.40	0.02
LMC136042	M3 I	3500	-8.54	4.83	3533	-32	-8.29	-0.25	1.07	3529	-28	-8.41	-0.13
LMC137624	M0 I	3700	-7.19	3.97	3792	-91	-7.01	-0.18	0.94	3710	-9	-7.16	-0.03
LMC137818	M2 I	3625	-7.57	4.46	3631	-5	-7.52	-0.05	1.07	3538	87	-7.90	0.33
LMC138405	M1 I	3675	-7.35	4.00	3781	-105	-7.11	-0.24	0.94	3710	-34	-7.24	-0.11
LMC140296	M2 I	3625	-8.22	3.90	3819	-193	-7.75	-0.47	0.96	3681	-55	-8.04	-0.18
LMC141430	M1 I	3700	-8.55	3.97	3792	-91	-8.37	-0.18	1.07	3533	167	-9.14	0.59
LMC142202	M1.5 I	3650	-8.36	4.19	3714	-63	-8.18	-0.18	0.95	3693	-42	-8.22	-0.14
LMC142907	M2 I	3650	-7.74	3.95	3799	-148	-7.39	-0.35	0.93	3732	-81	-7.49	-0.25
LMC143877	K3 I	3900	-8.58	3.00	4265	-364	-8.23	-0.35	0.78	4039	-138	-8.39	-0.19
LMC146126	K5 I	3875	-8.62	2.92	4313	-437	-8.19	-0.43	0.79	4008	-132	-8.43	-0.19
LMC147199	M1.5 I	3675	-7.82	4.75	3551	124	-8.18	0.36	1.10	3499	176	-8.49	0.67
LMC149721	M0 I	3750	-7.51	3.72	3893	-142	-7.28	-0.23	0.89	3797	-46	-7.39	-0.12
LMC157533	K5 I	3825	-7.00	3.81	3853	-27	-7.03	0.03	0.89	3806	19	-7.05	0.05
LMC158317	M1 I	3675	-7.45	4.12	3736	-60	-7.30	-0.15	0.97	3662	13	-7.49	0.04
LMC159974	K1 I	4300	-7.72	2.68	4473	-172	-7.50	-0.22	0.67	4315	-14	-7.72	0.00

Table 3—Continued

Star	Spectral Type	Spectral Fit ^a		Results from $(V - K)_0$					Results from $(V - R)_0$				
		T_{eff}	M_{bol}	$(V - K)_0^b$	T_{eff}	ΔT_{eff}^c	M_{bol}	ΔM_{bol}^d	$(V - R)_0^e$	T_{eff}	ΔT_{eff}^c	M_{bol}	ΔM_{bol}^d
LMC169754	K2 I	4100	-8.01	3.05	4232	-131	-7.92	-0.09	0.76	4086	14	-8.01	0.00
LMC174714	M1.5 I	3625	-8.39	4.05	3762	-136	-8.03	-0.36	0.96	3688	-62	-8.19	-0.20
LMC175464	M2 I	3625	-8.62	4.13	3734	-108	-8.32	-0.30	0.97	3672	-46	-8.47	-0.15
LMC175746	M3 I	3550	-8.35	4.43	3637	-86	-8.00	-0.35	1.04	3575	-24	-8.26	-0.09
LMC176890	M0 I	3750	-7.52	3.74	3885	-134	-7.32	-0.20	0.90	3779	-28	-7.45	-0.07
LMC177150	M1.5 I	3600	-7.26	4.38	3652	-51	-7.05	-0.21	1.05	3552	48	-7.44	0.18
LMC177997	M1.5 I	3675	-8.24	4.11	3740	-64	-8.08	-0.16	0.93	3727	-51	-8.09	-0.15

^aFrom Table 2.

^b $(V - K)_0 = (V - K_S) - 0.06 - 0.88A_V$.

^c ΔT_{eff} = Effective temperature adopted from spectral fitting the optical spectrophotometry *minus* the effective temperature determined from the broad-band colors.

^d ΔM_{bol} = Bolometric luminosity from spectral fitting the optical spectrophotometry *minus* the bolometric magnitude determined from the broad-band colors.

^e $(V - R)_0 = (V - R) - 0.19A_V$.

Table 4. Effective Temperature Scales

Spectral Type	SMC				LMC				Milky Way ^a			
	T_{eff} (K)	σ_{μ}^{b}	N	BC	T_{eff} (K)	σ_{μ}^{b}	N	BC	T_{eff} (K)	σ_{μ}^{b}	N	BC
K1-K1.5 I	4211	34	7	-0.73	4300	...	1	-0.70	4100	100	3	-0.79
K2-K3 I	4025	38	15	-0.92	4050	62	3	-0.80	4015	40	7	-0.90
K5-M0 I	3788	36	10	-1.27	3850	18	2	-1.09	3840	30	3	-1.16
M0 I	3625	19	5	-1.62	3738	11	4	-1.31	3790	13	4	-1.25
M1 I	3625	...	1	-1.61	3695	8	5	-1.45	3745	17	7	-1.35
M1.5 I	3654	14	6	-1.59	3710	8	6	-1.43
M2 I	3475	...	1	-2.07	3625	7	5	-1.69	3660	7	17	-1.57
M2.5 I	3545	13	5	-1.99	3615	10	5	-1.70
M3 I	3542	18	3	-2.01	3605	4	9	-1.74
M3.5 I	3550	11	6	-1.96
M4-M4.5 I	3450	...	2	-2.18	3535	8	6	-2.03
M5 I	3450	...	1	-2.49

^aFrom Paper I.

^bStandard deviation of the mean.

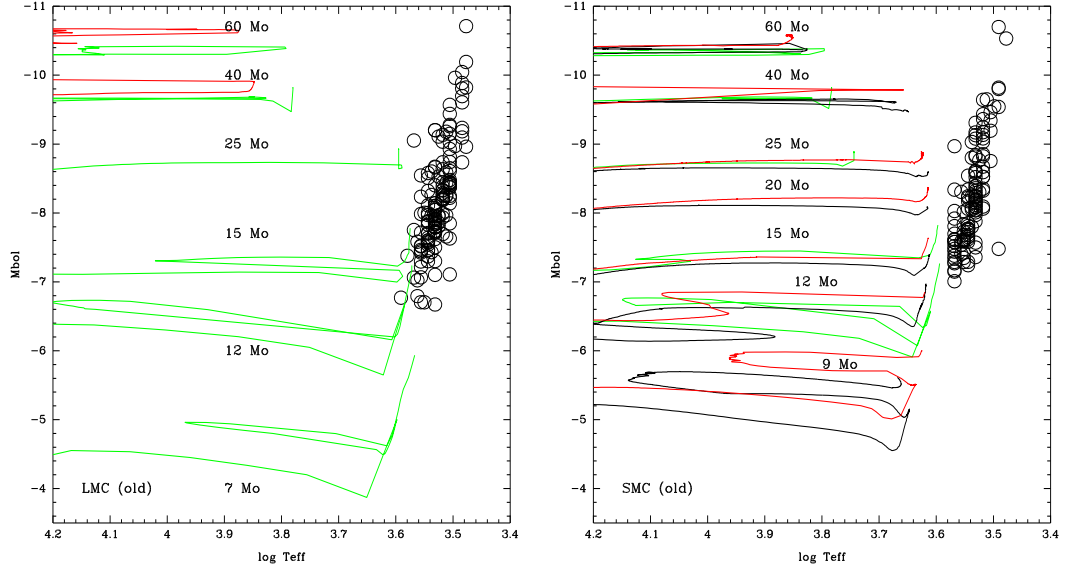


Fig. 1.— The location of Magellanic Cloud RSGs (from the literature) compared to the evolutionary tracks. This figure has been adapted from Massey & Olsen (2003), and shows the mismatch between modern evolutionary theory and the canonical locations of RSGs in the SMC and LMC, where the effective temperatures and bolometric corrections are based on those in the literature with a modest correction for metallicity (see Massey & Olsen 2003). The tracks do not produce stars as luminous and as cool as those “observed”. A similar problem for Galactic metallicity was solved by a significantly revised effective temperature scale based upon fitting the MARCS stellar atmosphere models to optical spectrophotometry. The older, non-rotation evolutionary tracks which include the effects of overshooting are shown in green, and come from Schaerer et al. (1993) for the LMC and Charbonnel et al. (1993) for the SMC. The newer evolutionary tracks (when available) are shown in black (zero rotation) and in red (300 km s^{-1} initial rotation), and come from Meynet & Maeder (2005) for the LMC, and Maeder & Meynet (2001) for the SMC.

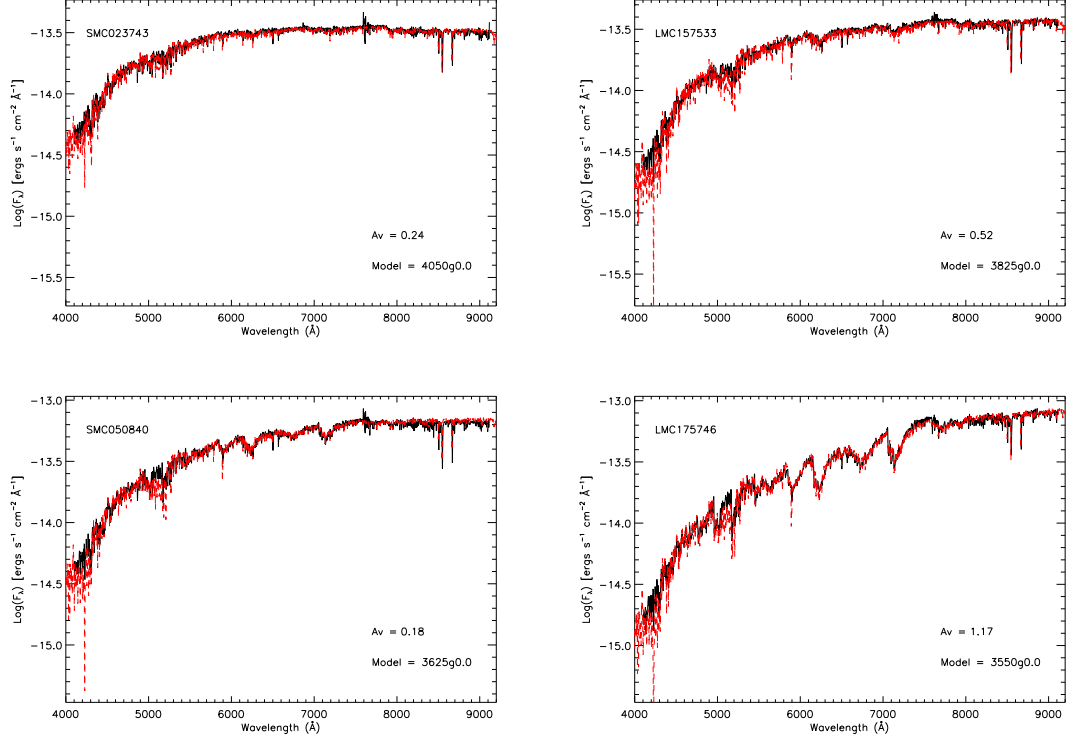


Fig. 2.— Model fits to optical spectrophotometry. The observed spectral energy distributions are shown in black, and the adopted model fits in red. The models have been reddened by the indicated amount using the standard $R_V=3.1$ reddening law of Cardelli et al. (1989). Four examples are shown here: SMC023743 (K2 I), LMC 157533 (K5 I), SMC050840 (M1 I), and LMC 175746 (M3 I). The individual fits are shown as Figures 2.2-2.76 in the electronic edition.

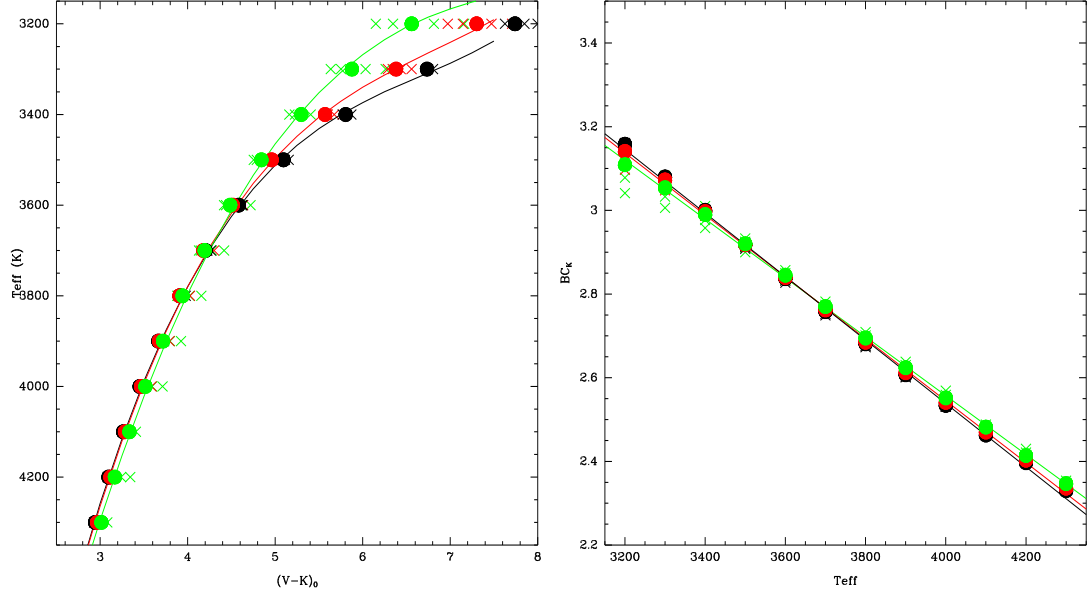


Fig. 3.— The transformation relations for K-band photometry. Black represents the results from the MARCS models with solar metallicity, while red represents the LMC and green the SMC. The filled circles show the values for $\log g = 0.0$, while the x’s cover the $\log g$ range from -1 to +1. The solid curves denote the fits from § 3.3.1. (a) Transformation between T_{eff} and $(V - K)_0$. (b) Transformation between BC_K (the bolometric correction at the K-band) and effective temperature.

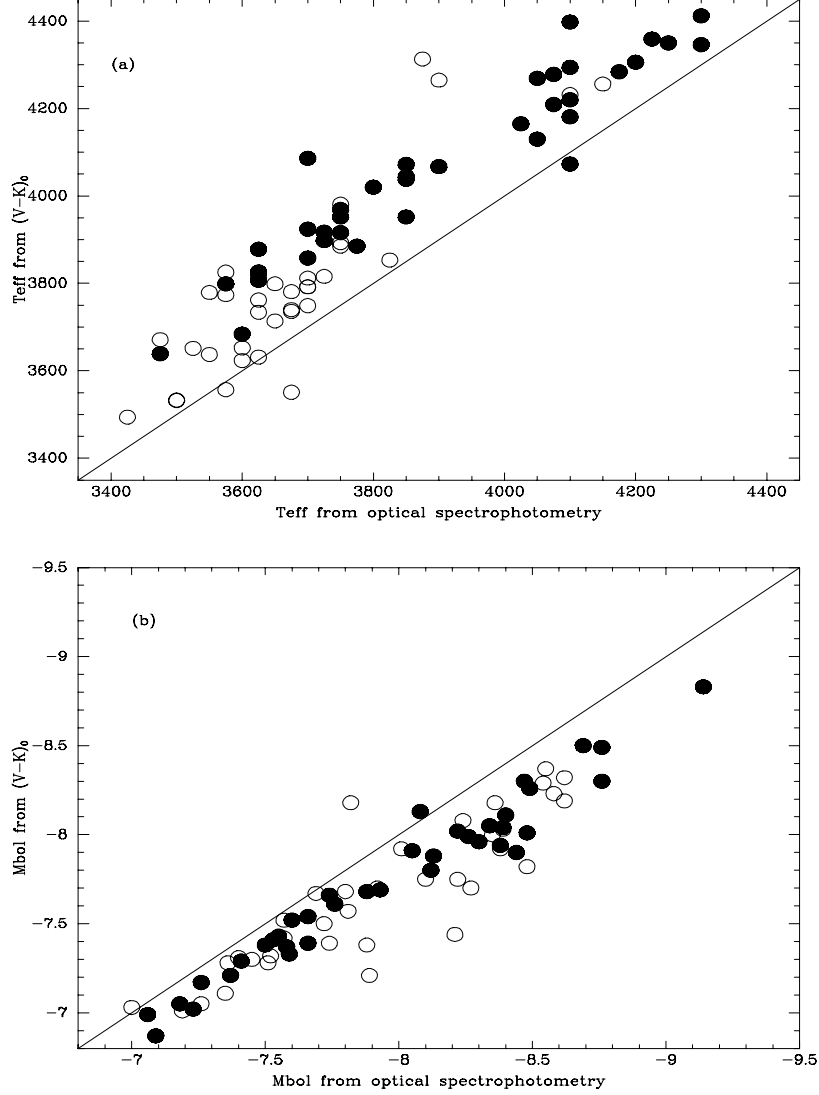


Fig. 4.— The physical properties derived from $(V-K)_0$ compared to those obtained by fitting the optical spectrophotometry. Filled circles show the data for the SMC, while open circles show the results for the LMC. The solid lines shows the 1:1 relation. (a) The effective temperatures T_{eff} found from $(V-K)_0$ are systematically higher than those obtained from the band depths of TiO when fitting the optical spectrophotometry. The median offset is -105 K (LMC) and -170 K (SMC). (b) The bolometric magnitudes are similarly affected, with a median offset of -0.23 mag (LMC) and -0.21 mag (SMC).

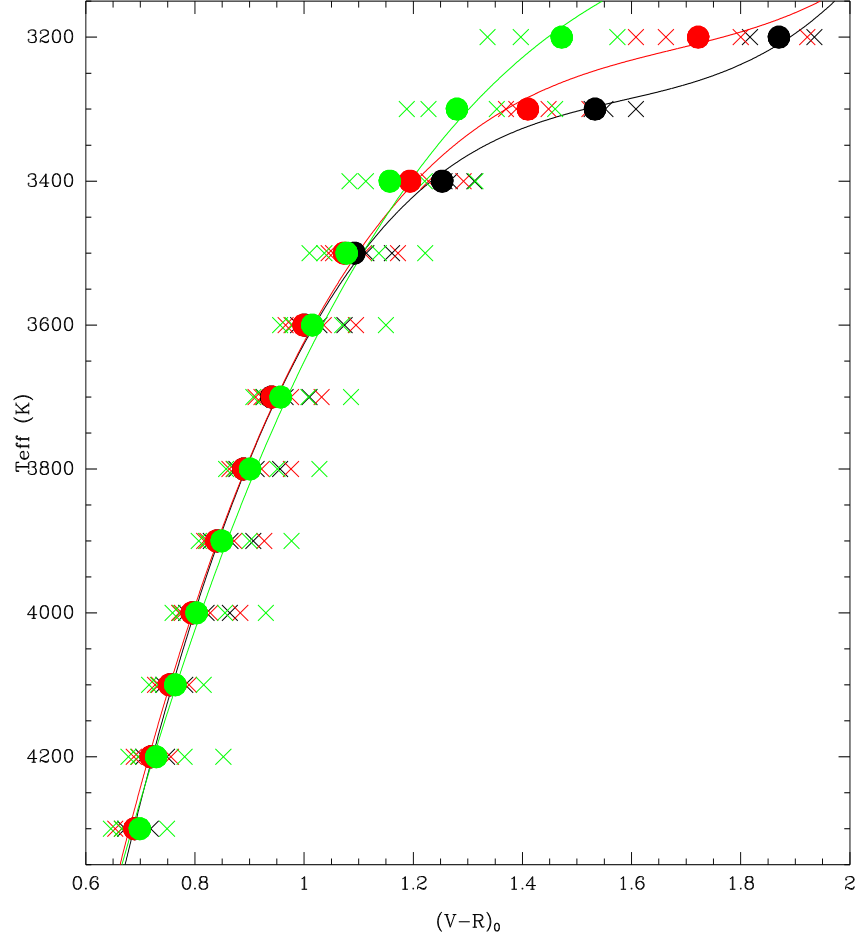


Fig. 5.— The transformation relation for $(V - R)_0$ photometry. Black denotes the Milky Way, red the LMC, and green the SMC. The filled circles show the values for $\log g = 0.0$, while the x's cover the $\log g$ range from -1 to +1. The fit was performed excluding the extremes in $\log g$, although these data are shown here.

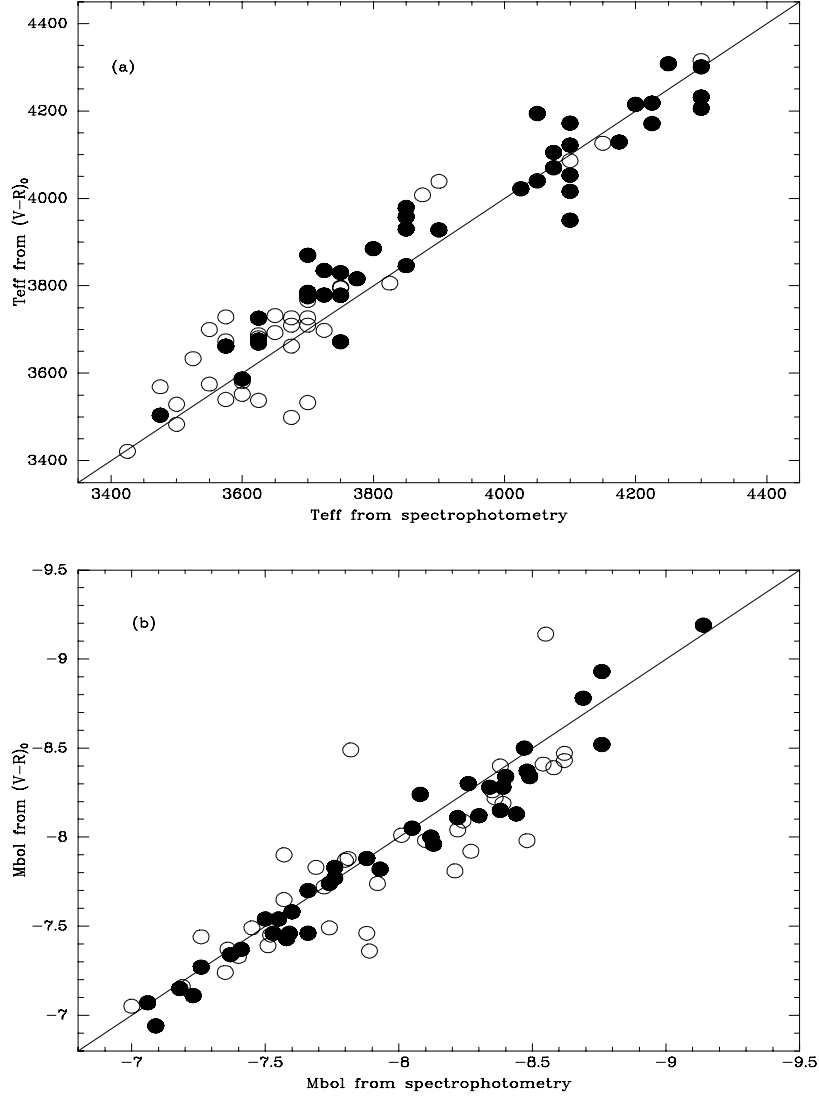


Fig. 6.— The physical properties derived from $(V-R)_0$ compared to those obtained by fitting the optical spectrophotometry. Filled circles show the data for the SMC, while open circles show the results for the LMC. The solid lines shows the 1:1 relation. (a) The effective temperature T_{eff} found from $(V-R)_0$ show no systematic difference for the LMC when compared to the values derived from optical spectrophotometry. The data show only a slight offset. The formal median differences are -30 K for both galaxies. (b) The bolometric luminosities computed using the $(V-R)_0$ colors to define the T_{eff} used for computing the bolometric corrections at V . As expected, the differences are slight, given the good agreement of the temperatures, with a median difference of -0.11 mag (LMC) and -0.04 mag (SMC).

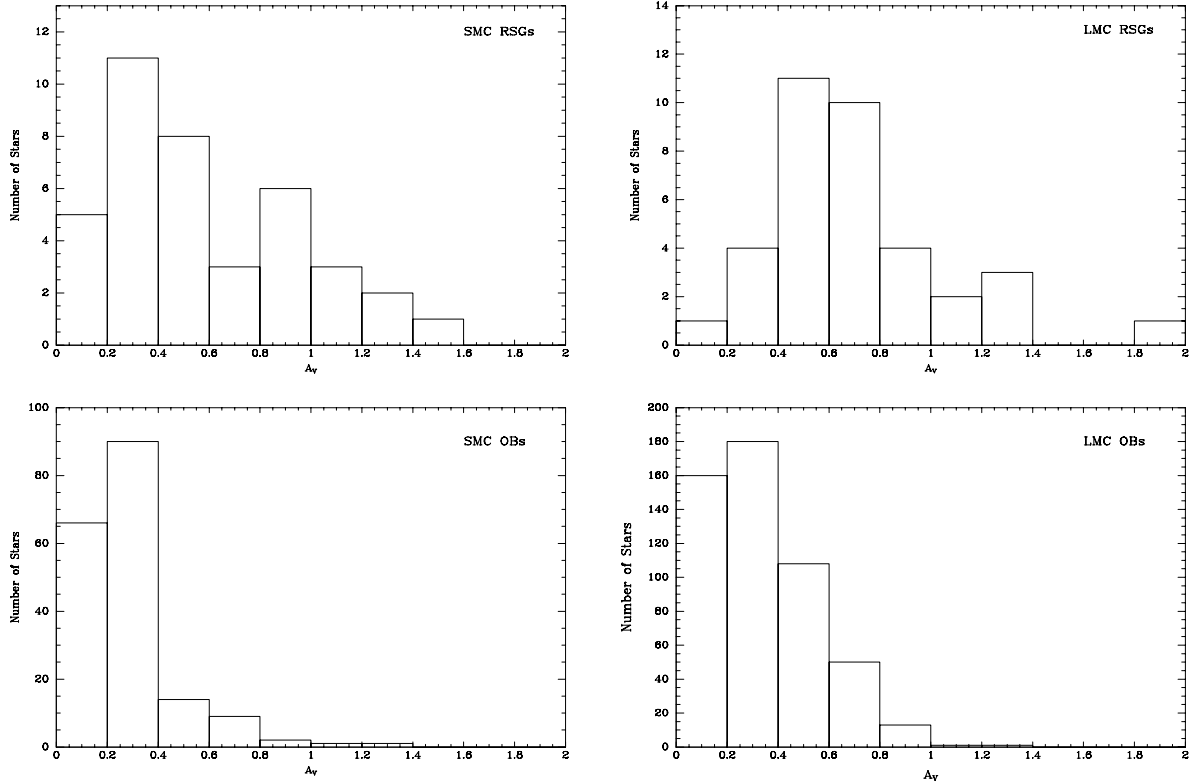


Fig. 7.— The distribution of A_V of RSGs is compared to that of OB stars. In both the SMC (left) and LMC (right) there is significantly more reddening for RSGs than is seen for OB stars. For the SMC the RSGs have $\bar{A}_V = 0.60 \pm 0.06$, compared to the OB stars, which have $\bar{A}_V = 0.24 \pm 0.01$. For the LMC, the RSGs have $\bar{A}_V = 0.73 \pm 0.06$ compared to the OB stars which have $\bar{A}_V = 0.32 \pm 0.01$. The errors quoted are the standard deviations of the mean. In addition, the distributions in A_V are considerably broader for the RSGs, as is obvious from the figure: the O stars have quite a narrow distribution in A_V , with $\sigma = 0.25$ for each Cloud, while the distribution for the RSGs is broader, 0.39 mag for each Cloud. This is consistent with our finding for the Milky Way (Paper I and Massey et al. 2005a).

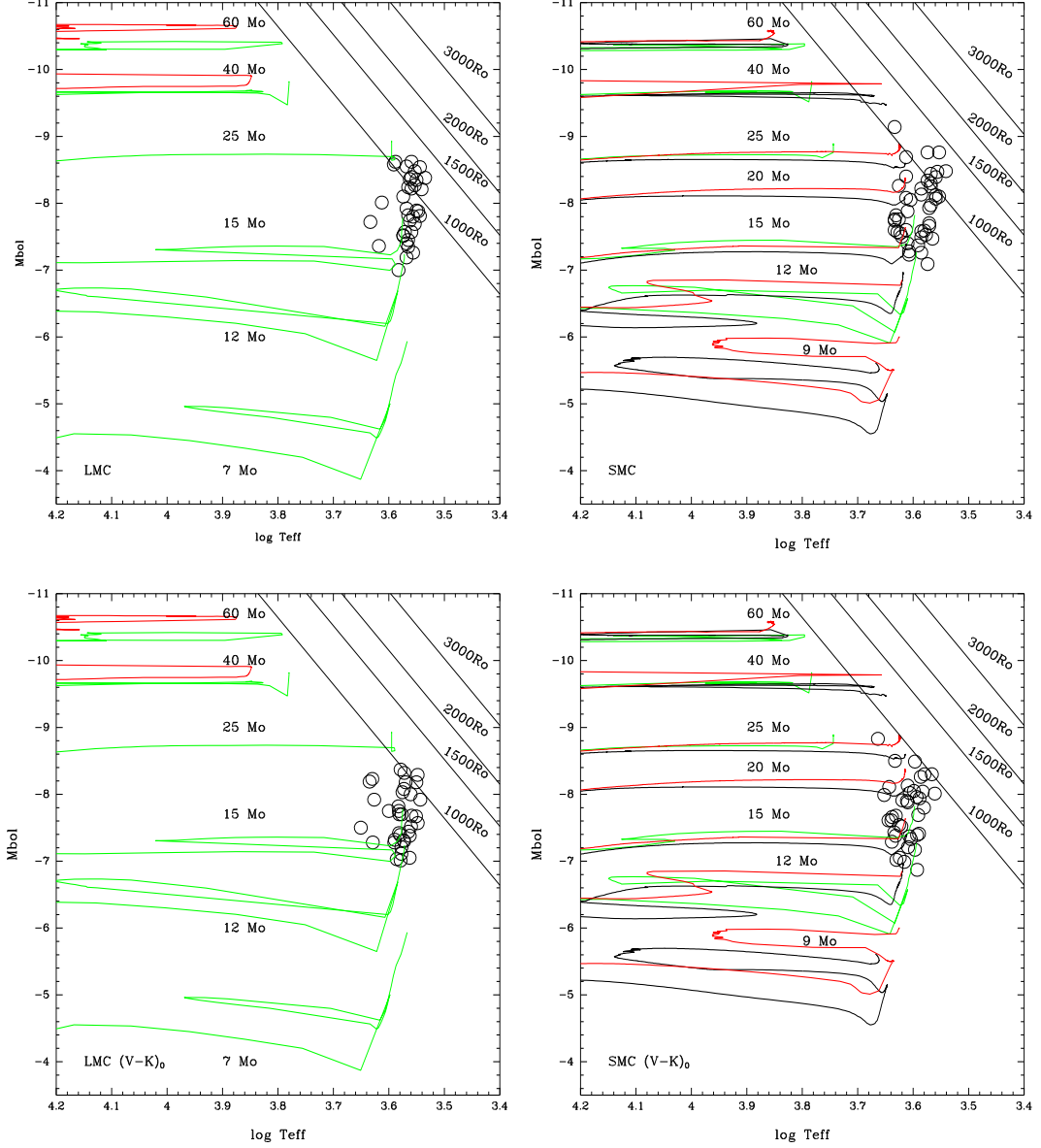


Fig. 8.— The location of Magellanic Cloud RSGs compared to the evolutionary tracks (this work). In the top two panels we show the location of the RSGs in the H-R diagram for the LMC (left) and SMC (right), where the effective temperatures and bolometric luminosities come from fitting the MARCS models to the optical spectrophotometry. Compare these to those shown in Fig. 1. The same evolutionary tracks are plotted here as in Fig. 1. The bottom two panels show the same locations as derived from the $(V - K)_0$ calibration.

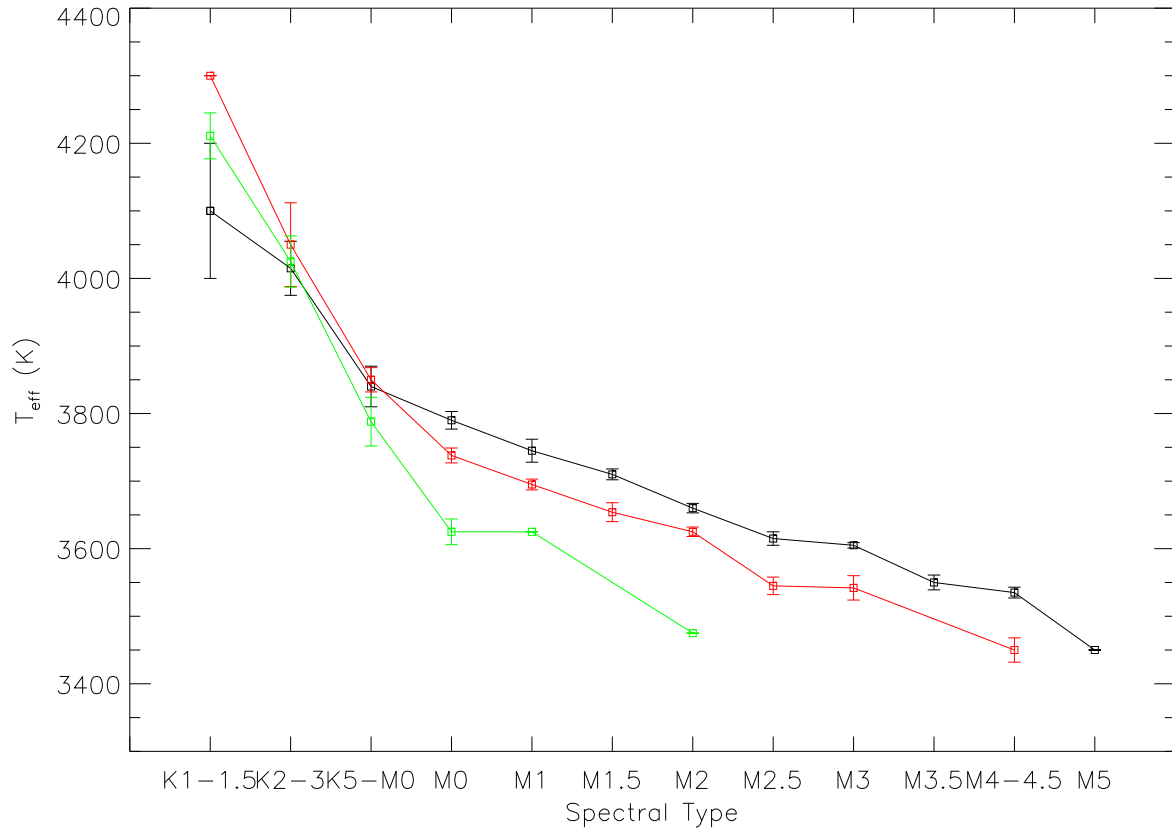


Fig. 9.— Effective temperature scales for Galactic (black), LMC (red), and SMC (green) RSGs. The error bars reflect the standard deviation of the means from Table 4.

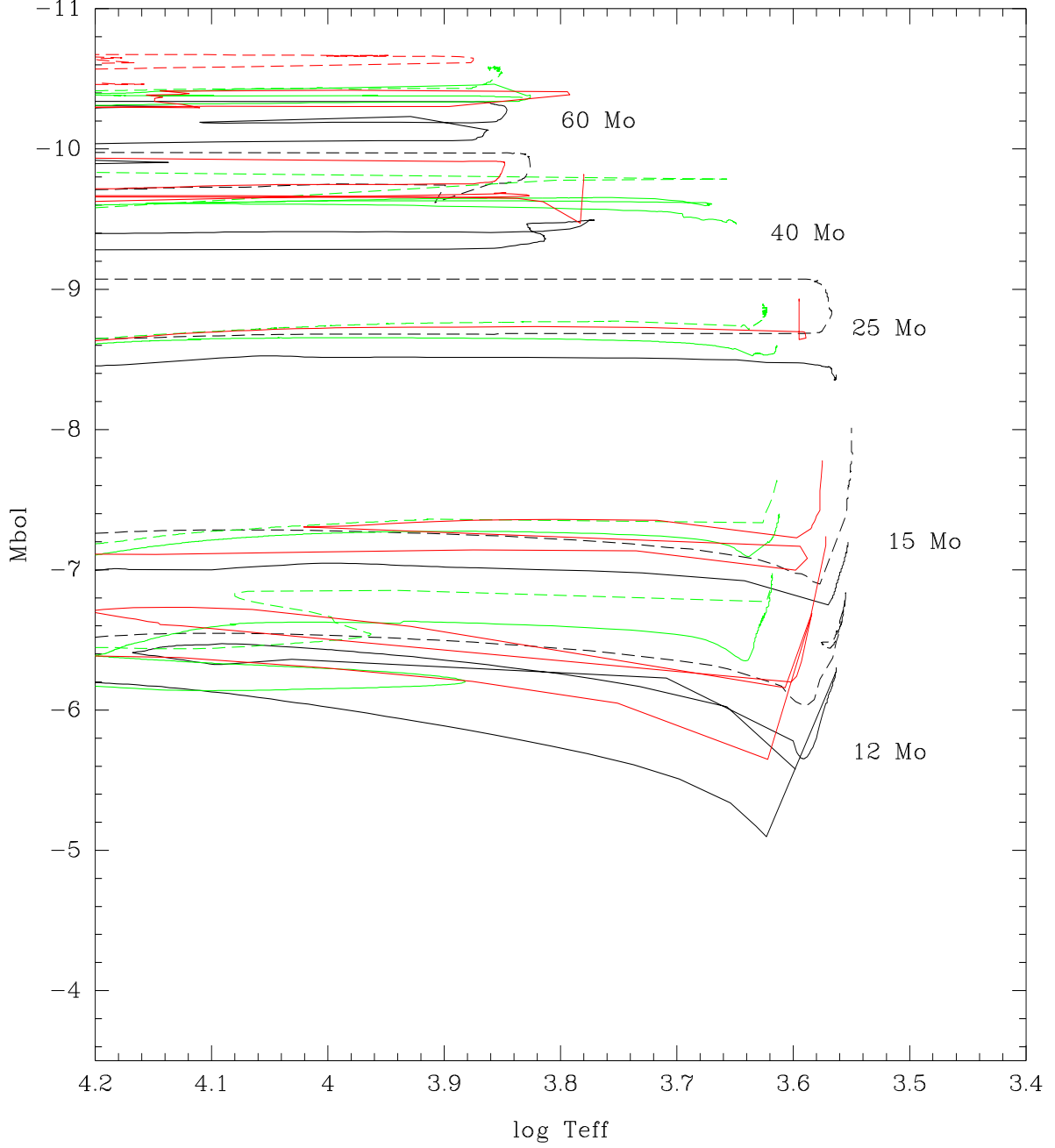


Fig. 10.— Comparison of evolutionary tracks at differing metallicities. We show the evolutionary tracks corresponding to the Milky Way (black, $z = 0.02$), the LMC (red, $z = 0.008$, and SMC (green, $z = 0.004$) from Meynet & Maeder (2001, 2005), Schaerer et al. (1993), and Charbonnel et al. (1993). Solid curves indicate no rotation, and dashed curves represent initial rotation velocities of 300 km s^{-1} .